

THERMAL CONTROLLED ELECTROCHEMICAL
INSTRUMENTATION FOR PROTEIN ARRAY
MICROSYSTEMS

By

Xiaowen Liu

A THESIS

Submitted to
Michigan State University
in partial fulfillment of the requirements
for the degree of

MASTER OF SCIENCE

Electrical Engineering

2011

ABSTRACT

THERMAL CONTROLLED ELECTROCHEMICAL INSTRUMENTATION FOR PROTEIN ARRAY MICROSYSTEMS

By

Xiaowen Liu

Understanding the structure and function of proteins has become increasingly important since the completion of the Human Genome Project and the sequencing of several other important genomes. In recent years, lab-on-a-chip systems have introduced some new capabilities for protein analyses. Rapid progress in the field of microsystems, miniaturized devices combining sensor and electronics, enable a new generation of miniaturized biosensor arrays integrating silicon CMOS chips that acquire and process bio-electrochemical signals. Such biosensor array microsystems could permit improved sensitivity, throughput and cost. Because many proteins exhibit temperature dependent activity, this thesis explores the opportunity to develop a thermal control microsystem for protein arrays biosensors. A CMOS microhotplate array was developed for thermoregulation of protein interfaces in a liquid sample environment. The microhotplates were shown to provide suitable thermal control for biosensor temperature ranges without the process complexity of most previously reported microhotplates. When combined with a CMOS analog thermal controller, the on-chip array was shown to set and hold temperatures for each protein site within $\pm 1^\circ\text{C}$, and array elements were found to be almost completely thermally isolated from each other at distances beyond 0.4mm. Furthermore, a new compact, low power impedance analysis circuit was developed utilizing mixed-mode signal processing to extract real and imaginary impedance components for an on-chip protein interface. The compact size and low power of this circuit enable it to be combined with the thermal control structures and instantiated for every element in a sensor array to increase the interrogation throughput. The developed thermal control and readout microsystem could significantly advance proteomics research and progress in characterizing newly sequenced genomes.

DEDICATION

Dedicated to my family

ACKNOWLEDGEMENT

The work presented in this thesis would not have been possible without the support, contribution, and encouragement of many individuals that I have had the privilege of interacting with during my stay at Michigan State University. Indeed this is now a unique opportunity to acknowledge them, even though in a very small way.

First, and foremost, I would like to express my deep gratitude to my advisor, Professor Andrew Mason, for his generous support. His broad vision and encouragement has always been a source of inspiration for me. His enthusiasm and wise criticism have had a tremendous influence on my professional development, which I am deeply grateful for.

I am also grateful to Professor Tim Hogan and Professor Shantanu Chakrabartty for serving on my committees. They have always been an exceptional source of support for me at MSU. Their technical feedback and original ideas greatly expanded the scope of my research and its contributions.

I am greatly indebted to all my colleagues and friends at MSU for their coaching and support in our joint entrepreneurial endeavors. Special thanks to Dr. Yang Chao, Dr. Huang, Yue, Dr. Awais M. Kamboh, Daniel Rairigh, Xiaoyi Mu, Haitao, Li, Yuning, Yang, Lin Li, Waqar A. Qureshi and Chenling Huang.

My utmost gratitude, love and affection belong to my family. My parents always unconditionally love and support me and I thank them for everything they have given me. I would like to thank my husband, Yang Liu, who accompanied me through the past years at Michigan State University. This thesis is dedicated to them.

TABLE OF CONTENTS

LIST OF TABLES	vii
LIST OF FIGURES	viii
LIST OF SYMBOLS	x
Chapter 1	1
Introduction.....	1
1.1 Motivation.....	1
1.2 Challenges.....	3
1.3 Thesis Goals.....	4
1.4 Thesis Outline	5
Chapter 2	6
Background.....	6
2.1 Protein Array Microsystems	6
2.2 On-Chip Thermal Control.....	7
2.2.1 Micro-hotplate Device	7
2.2.2 On-chip Temperature Controller.....	8
2.3 Protein Detection Circuits.....	9
2.4 Architecture of Protein Microsystem.....	11
Chapter 3	14
First Generation Micro-thermoelectric Control System	14
3.1 Thermal Control.....	14
3.1.1 Requirements	14
3.1.2 Architecture.....	14
3.1.3 Microhotplate Array Design	15
3.1.4 PID Thermal Controller	20
3.2 Microsystem Packaging.....	20
3.3 Measurement Results and Analysis	22
3.4 Summary and Analysis	26
Chapter 4.....	29
Impedance Extraction Circuits for Protein Array	29
4.1 Architecture of Impedance Extraction Circuits	30
4.2 Impedance Readout Circuit.....	31
4.2.1 Theory of Operation.....	31
4.2.2 IDC Circuit Implementation	33

Chapter 5	38
Second Generation Thermal Control Chip with Test Results.....	38
5.1 Second Generation Thermal Control Chip Design	38
5.1.1 Ambient Temperature Sensor Design	39
5.1.2 Thermal Controller Circuit Design	41
5.2 Test Results	46
5.2.1 Thermal Control Circuit Test Results	46
5.2.2 IDC Circuit Test Results	48
5.2.2.1 Circuit Characterization	48
5.2.2.2 Biosensor Measurements	53
 Chapter 6	 56
Summary and Future Work.....	56
6.1 Summary	56
6.2 Future Work	58
 BIBLIOGRAPHY	 61

LIST OF TABLES

Table 5-1. The performance of impedance-to-digital converter circuit.....53

LIST OF FIGURES

Figure 2.1. Schematic view and equivalent model of a two-electrode electrochemical site with a counter electrode (CE) and a gold working electrode (WE) coated with a tBLM. In the tBLM equivalent model, R_m and C_m represent the resistance and capacitance of the lipid bilayer membrane, respectively, while R_s is the resistance of the solution and C_{dl} describes the interfacial capacitance.....	10
Figure 2.2. Simplified schematic of a typical electrochemical potentiostat system. Normally three electrodes are employed: a working electrode, a reference electrode and a counter electrode.....	11
Figure 2.3. Conceptual view of the microsystem platform for a membrane protein biosensor array on CMOS	12
Figure 3.1. Block diagram of the micro-thermoelectric control system.....	15
Figure 3.2. Cross section of the CMOS microhotplate for thermal control of on-chip biosensor arrays	17
Figure 3.3. Thermal analysis simulations: (a) temperature probed on surface of the heater; (b) temperature probed on surface of chip.....	19
Figure 3.4. Die photograph of the 1.5x1.5mm microhotplate 3x3 array	21
Figure 3.5. Chip packaging flow: (a) chip in DIP40; (b) dispense SU8 2002 using a syringe; (c) soft baking, UV exposure and hard baking; (d) final SU8 reservoir; (e) PDMS cap on DIP40 package. Steps (b) and (c) are repeated 4 or 5 times until package is fully filled with SU8	22
Figure 3.6. The 1.5x1.5mm wire bonded first thermal CMOS chip encapsulated with SU8 2002. There are 3x3 microhotplate array in the chip.....	23
Figure 3.7. Thermal step response of the microhotplate thermal control system for 3 °C steps.....	24
Figure 3.8. Temperature (at on-chip sensor) in air and in liquid at different heater voltages	25
Figure 3.9. Current density of a NEST (NEST is a hydrophobic recombinant polypeptide comprising the catalytic domain (residues 727–1216) of neuropathy target esterase) biosensor at different temperatures.....	26

Figure 3.10. The sensor measured temperature vs. the distance from the heating source to the sensor	27
Figure 4.1. IDC functional blocks derived from the FRA method. The circuit extracts the imaginary portion of admittance when $S=1$ and real portion when $S=0$	32
Figure 4.2. Simplified lock-in impedance-to-digital converter structure. ϕ is the reference square wave.....	35
Figure 5.1. The concept of the second generation thermal control chip. The ambient temperature sensor block detects the temperature of whole chip. Thermal control block controls the temperature of each protein site locally. The IDC circuit characterizes the activity of the protein interface	39
Figure 5.2. The simplified schematic of the CMOS PTAT ambient temperature sensing circuit.	41
Figure 5.3. The schematic of second generation thermal controller. The comparator used to control switched is a hysteresis comparator to reduce thermal noise	43
Figure 5.4. The schematic of the amplifier used in the thermal controller	44
Figure 5.5. (a) Description of temperature independent reference voltage and current generator. (b) Schematic of the temperature independent reference generator.	45
Figure 5.6. Die photograph of second generation thermal control chip	47
Figure 5.7 The test result of voltage (a) and current (b) reference with temperature for 10 °C to 70 °C.....	48
Figure 5.8. The deviation between set point temperature (Temp_set) and measured temperature for 25 °C to 50 °C with gain=2 setting measured 180 second	49
Figure. 5. 9. Test platform for the IDC chip with biosensor equivalent circuit model.....	50
Figure 5.10. The real (circles) and imaginary (squares) results from the IDC circuit for the test setup shown in Figure 5.9 along with theoretical (expected) curve for comparison.	51
Figure 5.11. Measured DNL and INL curve of one IDC channel output when the sinusoid input amplitude was swept from 0 to 10nA. The maximum DNL and INL are 59.8dB and 50.2dB, respectively.....	52
Figure 5.12. Response of an IDC readout channel as the phase of the input signal is varied from -180° to +180° degrees. Input amplitude (30nA) and frequency (100Hz) are kept constant.	52

Figure 5.13. The test setup for the biosensor measurements using the IDC circuit.54

Figure 5.14. tBLM amplitude and phase measured by a commercial instrument (CHI 660 B) and by the fabricated IDC circuit at different frequencies.....55

LIST OF SYMBOLS

PID	Proportional integral derivative
PTAT	Proportional to absolute temperature
tBLM	Tethered bilayer lipid membrane

Chapter 1

Introduction

1.1 Motivation

Proteins are vital entities in human cells and are involved in nearly all body functions both in healthy and diseased individuals [1-3]. Proteins are used to support the skeleton, control senses, move muscles, digest food, and against infections and process emotions. Understanding the structure and function of gene products, that is proteins, has been increasingly emphasized since the completion of the Human Genome Project and the sequencing of several other important genomes. Because proteins are the targets for virtually all pharmaceutical drugs and for most diagnostics [1], proteins can be used in detecting disease and creating new treatments for health problems such as cancer, cardiovascular and neurological disorders. According to the American Cancer Society , there would be more than 7.6 million deaths caused by cancer in 2007 worldwide (about 20,000 cancer deaths a day) [4], deaths that could potentially be prevented by better understanding of proteins.

To understand the role of proteins in biological operations, typically referred to as proteomics, the characterization of protein structure and function is critical. Protein characterization has been used widely in drug discovery, development of biosensors, clinical and forensic analysis, and many other biomedical applications [5-8]. According to

a statement by Front Line Strategic Consulting, Inc. (San Mateo, CA), published in February, the proteomics market reached around \$2.68 billion in 2008, up 76% from an estimated \$1.52 billion in 2003 [9]. In recent years, researchers have seen an increased interest and investment in a more personalized approach to medicine, aided by better understanding of human proteins. This approach means that doctors can detect disease at a much earlier stage and select the right treatment for each patient. Also, it will enable earlier and more precise diagnosis, a necessity for selecting patients that actually might benefit from expensive and very targeted drugs that only work for specific small groups of patients [1].

Recently, high-throughput protein array methods have begun to be considered as the next-generation evolution of DNA microarrays, which allow rapid, direct and quantitative detection of a wide range of biomolecules [10, 11]. Protein array technology takes advantage of the fact that a large number of targets can be analyzed in parallel measurements with low sample consumption. The reduction of sample volume is of great importance for all applications in which only minimal amounts of samples are available. Furthermore, it is possible to perform comparative analyses of several different samples within a single array chip. For example, in medical research, all relevant immune diagnostic parameters of interest can be analyzed in parallel, which save cost and time.

Techniques for measuring protein activities and structure can be generally divided into two main groups, optical and electrochemical. Electrochemical biosensor is a molecular sensing device that intimately couples a biological recognition element to an electrode transducer. The principle for electrochemical biosensor transducers is that many chemical reactions produce or consume ions or electrons, causing some change in the

electrical properties of the solution, which can be sensed as measuring parameters. Electrochemical biosensors have played a major role in the move towards simplified testing, including home-use devices [12]. Furthermore, miniaturized, electrochemical biosensors hold great promise for minimizing size, and power in vital applications such as point-of-care diagnostics. In summary, electrochemical biosensors are promising candidates for the next generation of protein characterization platforms.

1.2 Challenges

To minimize reagent cost, the high throughput protein array for multiple analyte concentration measurement should be built in a tiny chip, with size around 1cm^2 . This requires the size of on-chip electrodes have to be very small because there are up to hundreds of on-chip electrodes in the protein array chip. The miniature size of the electrodes caused the biosensor reaction signals are really weak ($\sim\text{aA}$ - fA for sensing current), so it is hard to detect these sensing signals by off-chip instruments due to the low signal to noise ratio (SNR). The weak biosensor reaction signal is a main challenge for high throughput protein array microsystem. To solve the detection limitation, integrating the electrodes directly on the instrumentation chip could eliminate external connection noise, and through miniaturization, the limits of detection can be extended by improving the SNR [13].

Temperature plays a major role in sensitivity of protein-based sensors because protein activity typically doubles every 10°C in its biological temperature window [14]. Furthermore, reliability and lifetime of protein interfaces and test reagents can be greatly improved by keeping them at low temperature as long as possible. However, to our best

knowledge, no protein array associated with thermal control microsystem was presented. The main challenge of this thermal controlled microsystem is to maintain the entire system, including valuable biomolecules, at a low temperature and only heat the protein site locally in liquid environment. To solve this challenge, an on-chip thermal control circuit, allowing temperature control each protein site individually, was expected.

1.3 Thesis Goals

The primary goals of this research are to develop the thermal control capabilities and instrumentation circuits that will permit the realization of a single chip, high throughput protein array microsystem. These two areas are described in detail below.

A: Thermal Control for Protein

To keep the protein platform at a low temperature and only heat the sensor site locally in liquid, a thermal controlled protein microsystem was proposed. In this thermal control system, several requirements need to be considered. First, the on-chip heaters and sensors have to be compatible with a standard CMOS process. Second, thermal uniformity across the microhotplate is needed to ensure no local hot spots will degrade the biointerfaces. Third, a feedback controller is needed to allow individual array sites to be set for different temperatures simultaneously. Forth, an in-package encapsulation system was also needed to verify thermal control operations in liquid environment necessary for protein-based interfaces.

B: Readout Circuits

Another circuit that is necessary in the protein array microsystem is the readout circuit that will sense and extract biosensor reaction signals. Because of the high level of integration in the microsystem, multi-channel readout circuits have to be hardware and power efficient. Furthermore, because the biosensor outputs are small signals, high resolution is another key requirement for the readout circuits. In summary, to support chip-scale microsystem applications, a very hardware efficient and low power solution is needed that combines accurate, low noise readout circuits with electronics capable of circumventing the heavy signal processing load involved in parallel sensing of a sensor array

1.4 Thesis Outline

In this thesis, Chapter 2 covers the background of protein array microsystem, on-chip thermal control and biosensor signal readout circuits. Chapter 3 covers the first generation of thermal control chip for protein array microsystem. It introduces the design concept of the microhotplates in standard 0.5 μm CMOS process and shows results that characterize the thermal performance in liquid. Chapter 4 describes a readout and impedance extraction circuit for protein characterization that introduces in a new structure for impedance extraction based on the frequency response analyzer (FRA) technique. Chapter 5 covers the second generation thermal control and readout chip and summarizes the chip performance and test results with a bilayer lipid membrane protein biosensor. Chapter 6 summarizes the thesis work, contributions and outlines future work related to this research.

Chapter 2

Background

2.1 Protein Array Microsystems

In recent years, miniaturized systems called lab-on-a-chip or micro total analysis systems (μ -TAS) have been introduced as new microsystems for biochemical analyses. These systems are expected to perform DNA, protein, and cell analyses for drug screening and development of novel therapies [15]. Microarray and microfluidic types of chip-scale devices (so-called biochips) have been developed using micro- and nano-technology techniques [15, 16]. These miniaturized biosensor arrays provide tremendous advantages. To fully realize these advantages, a microsystem that combines the biosensor microarray with miniaturized interrogation instruments is of increasing interest.

Several protein microsystems have been reported. In [17] an amperometric electrochemical microsystem for a miniaturized protein biosensor array was introduced. In [18], an integrated multi-channel impedance extraction circuit for biosensor arrays was developed, and a platform for detection of avian influenza was reported in [19]. However, none of these consider the environment temperature around the protein. To improve the sensitivity and reliability of the biosensor system, and reduce the cost, a new thermal controlled protein microsystem was developed, which was introduced in Section 2.4.

2.2 On-Chip Thermal Control

An on-chip temperature-controllable platform is of great advantage in sensor research into temperature-dependent phenomena. Most of the known on-chip thermal control systems were built for gas sensor [20-24]. The standard on-chip thermal control system includes two parts, a micro-hotplate device and a thermal controller.

2.2.1 Micro-hotplate Device

Using CMOS technology to generate a resistive heating element and a temperature sensor is generally called a *micro-hotplate*. In the microhotplate, most of the existing heating elements work as a resistive heater where an electrical current is applied to control temperature. The heating element can be made of any conductive material such as metal layers [23], polysilicon layers [21, 22], or transistors [20] within a CMOS process. The temperature sensing element can be resistive thermometers or NPN transistors realized as parasitic devices in a standard CMOS process [25-27].

Beginning in the early 1990s, the silicon micromachining was used to fabricate microhotplates and arrays for gas sensors. Numerous micro-hotplates have been produced by both surface [28] and bulk etching of silicon [29, 30]. Most of gas sensors demand post-CMOS processing (bulk etching, etc.) to remove silicon beneath of the hotplate and improve thermal isolation in air [31-33]. Many papers reported how to fabricate suspended membranes or microbridge structures for thermal isolation [21, 33], which are necessary to achieve temperatures around hundreds of degree Celsius (~200-600 °C).

However, in microhotplates designed for protein biosensor microsystems, the microhotplates will be heated in a liquid environment and the maximum temperatures are much lower, ~ 60 °C, than gas sensors. The thermal conduction and convection of a microhotplate in fluid are totally different than one in gas (e.g. air) and are mainly determined by the geometry and material of microhotplates. In Chapter 3, how to improve the temperature gradient and the heat transfer of microhotplate in liquid will be discussed further. Moreover, because the maximum temperature for protein sensors is much lower than that of gas sensors, the post-CMOS etching steps to create thermal isolation of the microhotplate are not necessary.

To our best knowledge, the only microhotplate designed for biological applications and used within liquid environments with no post-CMOS processing was reported for cell culture and incubation [21]. This device achieved a single fixed temperature of 37 °C on the back side of a CMOS chip. However, the protein array application requires programmable control of individual sites across a wide temperature range, which can not be achieved with the reported device. Thus, there are no reported devices suitable for the goals of this thesis research.

2.2.2 On-chip Temperature Controller

A classical temperature controller can be implemented using either analog or digital methods. In [33-36], temperature controllers were built based on the digital proportional-integral-derivative (PID) technique. The drawback of this method is that it requires a

large amount of hardware because it requires analog-to-digital and digital-to-analog converters plus anti-aliasing and smoothing filters within the thermal controller [35].

Analog temperature controllers have been around for many years, and there is a great deal of literature, practical experience, and design methods available. In [24, 37], analog temperature controllers based on Wheatstone bridge were used to detect the small variations in the resistive value of a temperature sensor resistor. [38, 39] introduced other analog temperature controllers to directly detect the temperature sensor resistor. Compared to a digital temperature controller, the analog thermal controller is more sensitive to the process variations and temperature drifts, but it simpler and needs fewer components.

2.3 Protein Detection Circuits

Impedance spectroscopy (IS) is a standard technique for protein identification and characterization. Protein bio-interfaces elicit responses that are measured by a change of impedance over a range of stimulus frequencies. The basic concept of the electrochemical IS (EIS) method is shown in Figure 2.1. A potentiostat imposes a desired command voltage between the solution and the working electrode while simultaneously measuring the current flowing between them those results from the applied voltage. The command voltage for impedance sensing is an AC excitation plus an optional DC offset, and the impedance is simply the ratio of the AC voltage to the AC response current. EIS analyzers are potentiostats designed especially for measuring AC impedance, and they have typical frequency ranges of 1 mHz – 100 kHz.

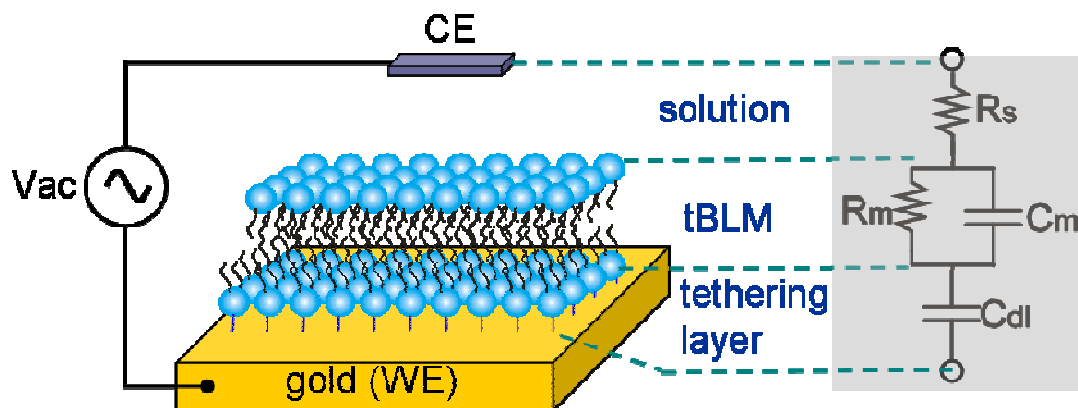


Figure 2.1. Schematic view and equivalent model of a two-electrode electrochemical site with a counter electrode (CE) and a gold working electrode (WE) coated with a tBLM. In the tBLM equivalent model, R_m and C_m represent the resistance and capacitance of the lipid bilayer membrane, respectively, while R_s is the resistance of the solution and C_{dl} describes the interfacial capacitance. (For interpretation of the references to color in this and all other figures, the reader is referred to the electronic version of this dissertation.)

Recently, some chip-level approaches for IS have been introduced [40, 41], but these lack the ability to extract real and imaginary impedance components. Impedance component extraction is necessary to identify sensing elements within the complex impedance (see model in Figure 2.1) and is essential for reducing the signal processing load in array implementations. A chip with impedance extraction and stimulus signal generation has been reported [42], but it utilizes an external DSP for output digitization and supports frequencies and current ranges that are not appropriate for membrane proteins.

Electrochemical amperometry techniques, such as cyclic voltammetry, are also often employed to characterize protein properties. As shown in Figure 2.2, one of the basic components of this electrochemical system is the potentiostat, a circuit that controls the bias voltage between two conductive electrodes, i.e. reference electrode (RE) and

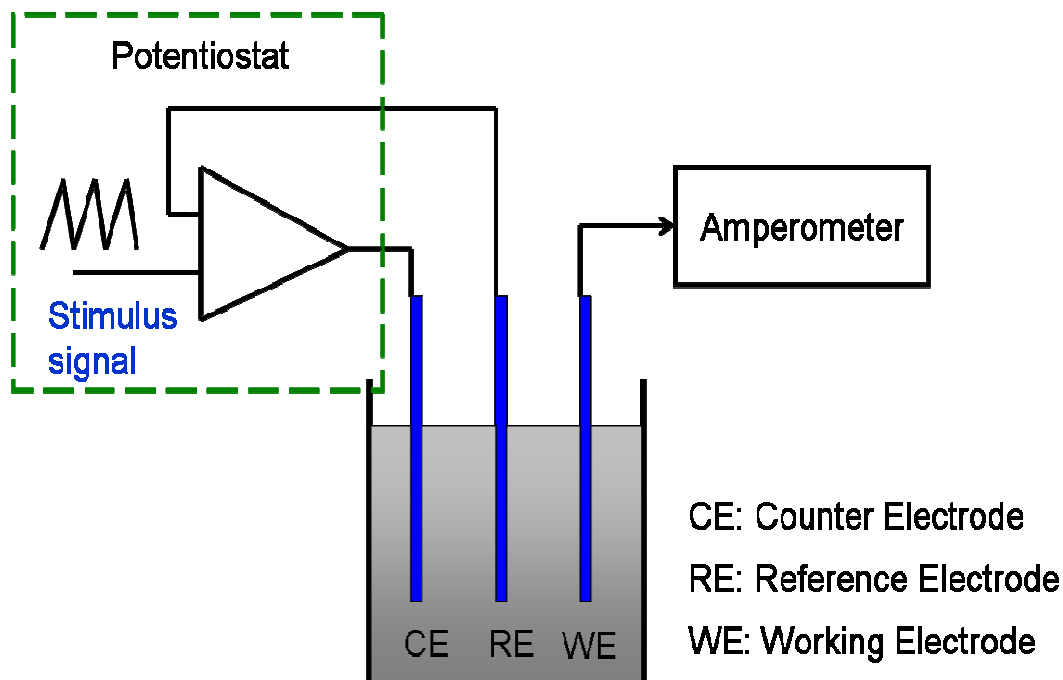


Figure 2.2. Simplified schematic of a typical electrochemical potentiostat system. Normally three electrodes are employed: a working electrode, a reference electrode and a counter electrode.

working electrode (WE). The electrical current between the counter electrode (CE) and the WE is then measured using an amperometric readout circuit [43].

Both EIS and amperometry techniques can be implemented with CMOS instrumentation circuits. For example, CMOS readout electronics including a compact potentiostat that supports a very broad range of input currents, 6 pA to 10 μ A, have been reported [17]. In another example, a CMOS bi-potentiostat and amperometric readout chip has been reported by our lab [44].

2.4 Architecture of Protein Microsystem

Figure 2.3 illustrates the proposed protein-based electrochemical biosensor array microsystem that serves as the conceptual model for the work described in this thesis. A silicon chip with CMOS electrochemical instrumentation circuitry forms the substrate. The circuitry includes on-chip thermal control and readout circuits to detect the biosensor reaction signal. The electrodes are individually modified with protein interfaces using molecular self assembly processes [14]. The assembly and measurement of biointerfaces are supported by a top microfluidics layer that could take a variety of forms including fluidic channels or, as shown in Figure 2.3, fluidic reservoirs that are filled and emptied by a robotic fluid delivery system. This platform is versatile and also permits electrode modification with other types of interfaces, such as redox enzymes. To interface the chip with biosensors, the chip needs to be suitably packaged for use in a liquid environment. The post-CMOS fabrication process begins with formation of electrodes by depositing titanium/gold ($50\text{\AA}/1000\text{\AA}$) on the CMOS chip and patterning by wet etch. A robust and reliable packaging scheme for on-CMOS biosensors that is uniquely capable of providing

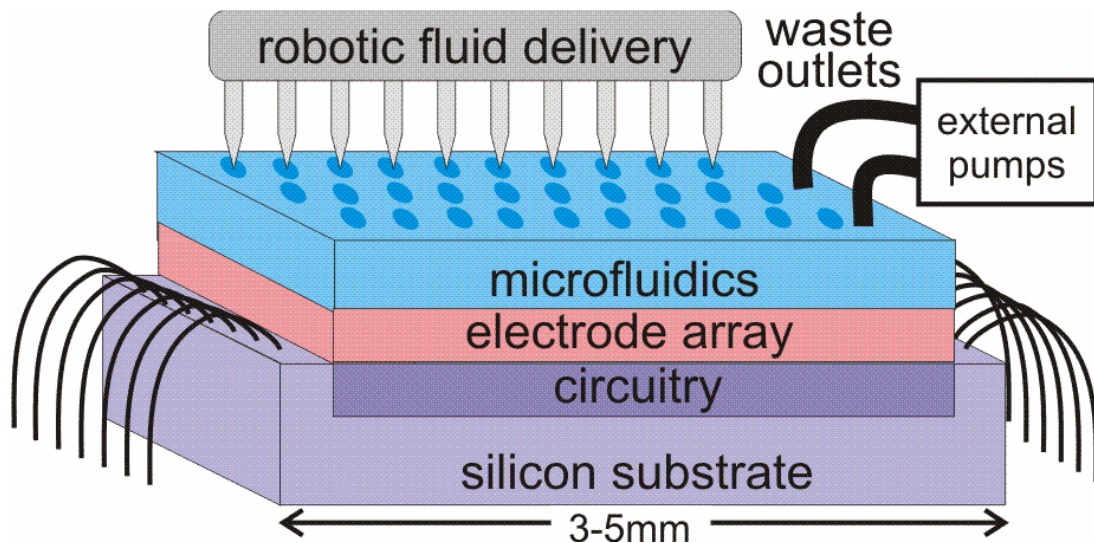


Figure 2. 3. Conceptual view of the microsystem platform for a membrane protein biosensor array on CMOS.

both electrical insulation of a CMOS chip in a liquid environment and also protection from chemical and biological agents has been developed by our lab [45].

Chapter 3

First Generation Micro-thermoelectric Control System

3.1 Thermal Control

3.1.1 Requirements

Most of the published microhotplates have been designed for gas sensing, where the temperature required several hundreds of degree Celsius. However, biological application have significantly different requirements including: lower temperature range suitable for protein characterization [46]; ability to control array sites to different individual temperatures; thermal uniformity across the microhotplate to ensure no local hot spots that would degrade the biointerfaces; no post CMOS thermal isolation; and a simple package that enables liquid to get to the chip surface without interfering with wire bond connections. This chapter describes efforts to develop a new thermal control system that will provide these functional characteristics.

3.1.2 Architecture

To control the temperature around a protein, an on-chip heater, temperature sensor, temperature controller, and protein-based interfaces are needed. A multi-channel thermal

control system, shown in Figure 3.1, was developed to characterize the performance of the on-chip microhotplate in a liquid environment. The microhotplate array utilizes a standard 0.5 μm CMOS process and requires only a 5V supply. A simple in-package encapsulation scheme was implemented to verify thermal control operations in a liquid environment necessary for protein-based interfaces.

To individually control the temperature of biointerfaces on the surface of a CMOS chip, each channel includes microhotplate and a feedback network for temperature control. The microhotplate is composed of a resistive heater, a resistive temperature sensor, heater driver circuitry, and sensor readout circuitry. A temperature-independent current, I_s , generates a proportional-to-temperature voltage that is read by an A/D converter. The proportional integral derivative (PID) thermal controller compares the expected

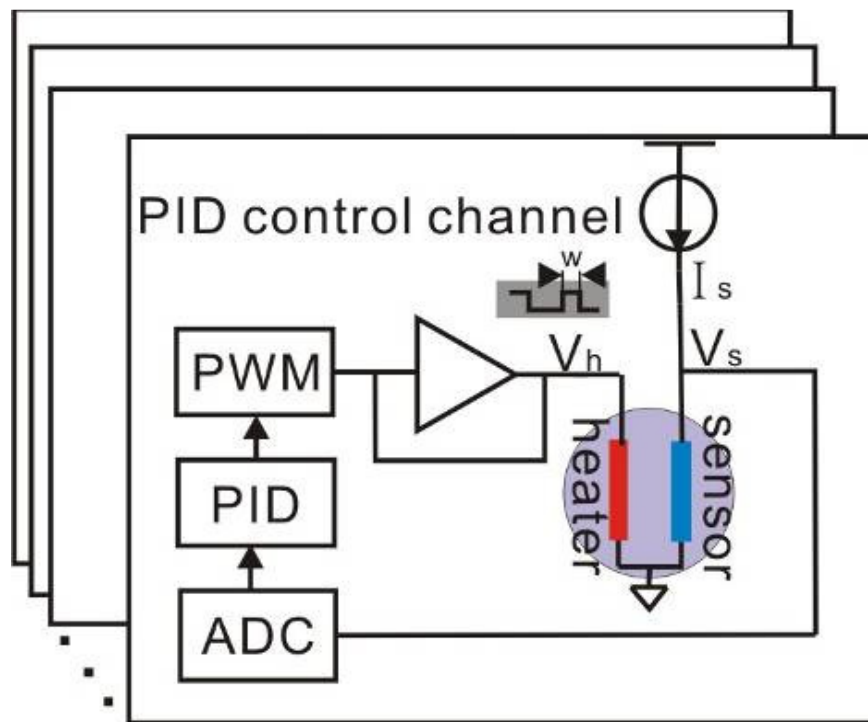


Figure 3. 1. Block diagram of the micro-thermoelectric control system.

temperature with the sensor-measured temperature and adjusts the duty cycle of the pulse width modulator (PWM). The PWM controls the heater to deliver the average power necessary to maintain the desired temperature. Because the heater and sensor are very near the surface of the chip, the temperature of the surface biointerface can be well maintained.

3.1.3 Microhotplate Array Design

A microhotplate is a micro-scale structure consisting of a heater and a temperature sensor and has been widely employed in gas sensors [21, 22, 33]. To adapt microhotplates to protein interfaces, significant prior work in modeling [47] and experimental design [48, 49] has been completed by past students in our lab. Building on these past efforts, to better understand the thermal behavior of this micro-scale thermal system, the microhotplates were modeled and simulated using the CoventorWare finite element analysis tool with the Electromagnetics and Heat Transfer modules. Design optimizations were performed based on the following requirements: ability to achieve temperatures near 45 °C, high thermal uniformity across the hotplate to prevent damage to biointerfaces, low power consumption, high thermal strength to increase robustness, and compatibility with a standard IC process. The finite element simulation results demonstrated that, when properly designed, a standard CMOS microhotplate 1) could be designed using two polysilicon layers for a heater resistor and a resistive temperature sensor as shown in Figure 3.2, and 2) could achieve the target temperatures (up to 45 °C) using only a 5V supply and without any post-CMOS etching of silicon beneath the microhotplate to improve thermal isolation. Furthermore, simulations showed that sufficiently high temperatures could be achieved even in the presence of a liquid environment. These

results are significant because they validate a new approach that has many potential advantages but has never been attempted or reported in the literature.

The microhotplate array was designed in the standard AMI 0.5 μm 3-metal, 2-poly CMOS process. As shown in Figure 3.2, the poly1 layer was used as the heater because of its high thermal capacity than metal layers and lower resistance compared to the poly2 layer. A circular design was chosen to reduce the heat dissipation [46]. To decrease resistance, and thus increase the maximum power delivered for a fixed voltage, concentric rings were chosen rather than a single serpentine heater. For a typical 100 μm diameter heater, the nominal heater resistance was 140 Ω , which provides sufficient heating using only a 5V supply. A thermal simulation of this structure is shown in Figure 3.3 (a). Notice the hotter areas where current density is higher. Due to the small diameter of the heater and the desire to keep resistance low, there is a limit to how well hot spots can be

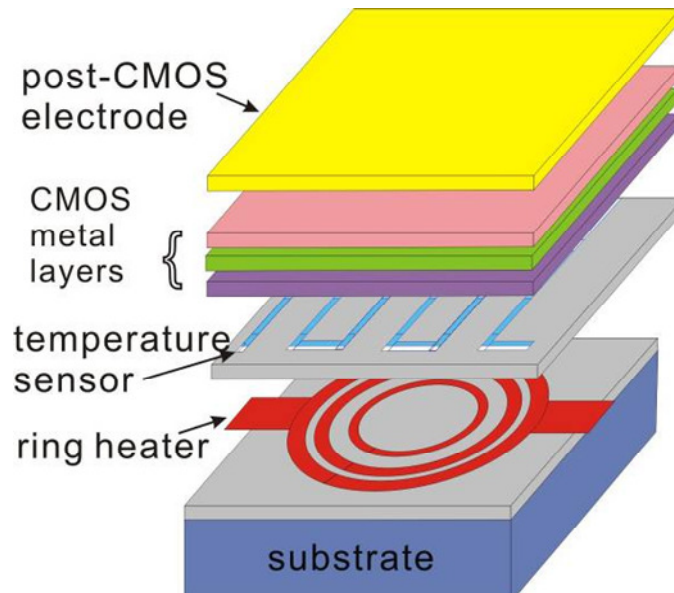
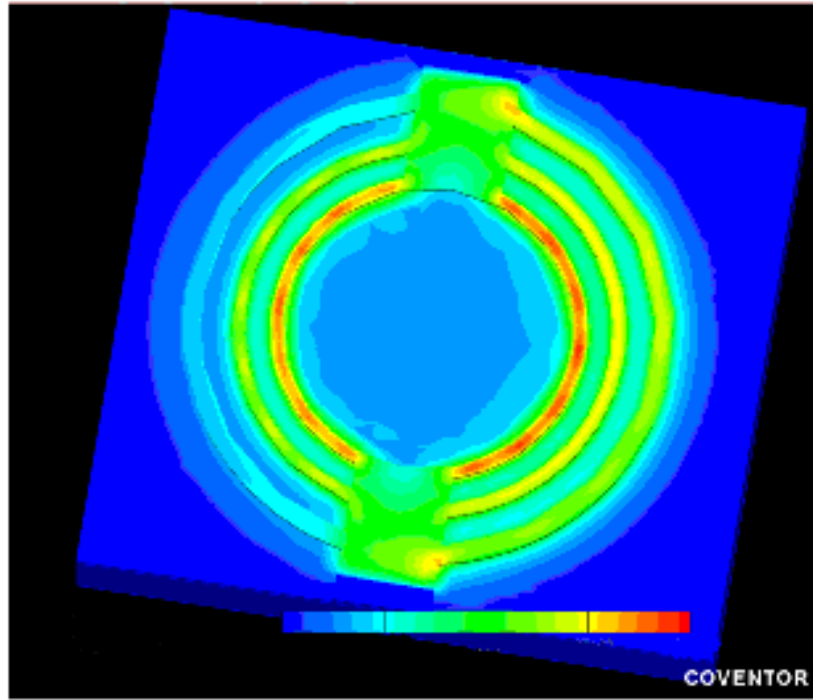


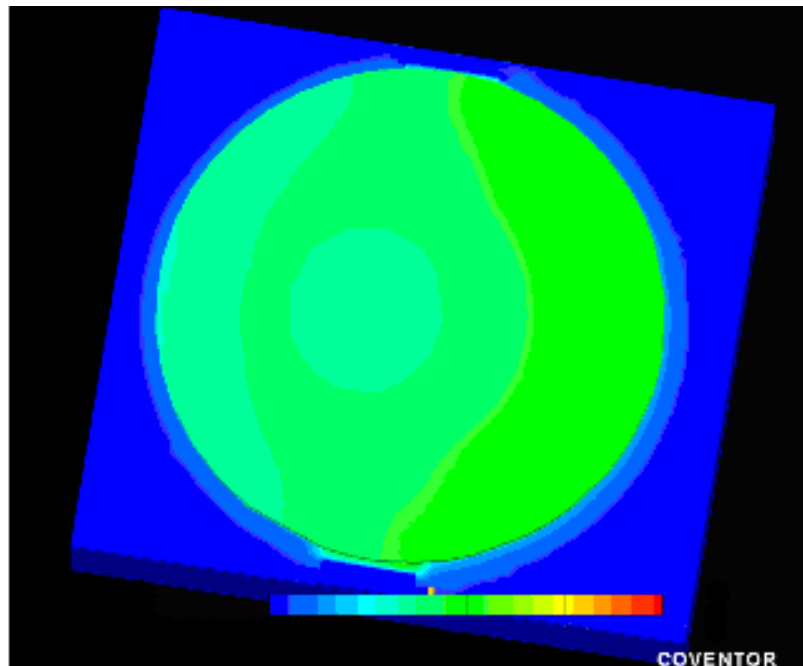
Figure 3.2. Cross section of the CMOS microhotplate for thermal control of on-chip biosensor arrays.

controlled just by changes in the poly1 layout. However, it was determined that proper allocation of highly thermally conductive CMOS metal layers and via contacts between the heater and the surface electrode could minimize the lateral thermal gradient [46] and remove all local hot spots, as shown in Figure 3.3 (b).

The final element of the microhotplate is the resistive temperature sensor, which was formed in poly2 because of its high sheet resistance and close proximity to the poly1 heater layer. The sensor resistor was laid out in a thin-wire serpentine pattern to average temperature across the heater area and produce a large resistance, nominally 300-400 k Ω .



(a)



(b)

Figure 3.3. Thermal analysis simulations: (a) temperature probed on surface of the heater; (b) temperature probed on surface of chip.

3.1.4 PID Thermal Controller

High precision in the thermal control system is desirable to ensure that all sensing processes on the microhotplate take place at the desired temperature throughout a measurement cycle. The PID controller is a well known structure that corrects the error between a measured variable and the desired setpoint. It calculates and then outputs a corrective signal to rapidly adjust the process and minimize error. By optimizing the P, I and D parameters for a microhotplate system, a high speed thermal controller with very small error was realized. In this prototype system, the PID controller was implemented in software. An analog feedback controller with similar functionality was designed for the next generation system described in Chapter 5.

3.2 Microsystem Packaging

A 3×3 microhotplate array with on-chip drive and readout circuitry was fabricated in 0.5µm CMOS and is shown in Figure 3.4. The chip was wire bonded to a standard DIP40 package for electrical testing. A simple packaging scheme that circumvents photolithography and enables liquid to get to the chip surface without interfering with wire bond connections was developed by lab mate Lin Li [45, 50]. This packaging scheme was adopted to conduct thermal tests in a liquid environment. The area around the chip and inside the DIP40 package was filled with SU8 photoresist. SU8 is commonly used to construct microstructures because it can form thick layers and is available in a wide range of viscosities. Experiments were performed to determine which viscosity of SU8 provided

the ideal combination of uniform coverage of the large package volume with sufficient surface tension to deter spreading onto the surface of the chip. SU8 2002 was found to be most effective. SU8 also provides thermal insulation for the chip, resulting in reduced heat loss to the ambient air. The SU8 was applied through a syringe in several layers, soft baking on a hotplate and cross linking with UV light after each layer, as shown in Figure 3.5.

After the final SU8 layer, isolated the wire bonds were isolated and created a reservoir of approximately 0.5 ml was formed above the chip, as shown in Figure 3.6. To extend the volume, a polymethylsiloxane (PDMS) cap was fabricated using an SU8 master and soft lithography standard for this the biocompatible PDMS material. The cap extended the height of the reservoir by about $400\mu\text{m}$, increasing the volume to approximately 1ml. The PDMS structure on the SU8 chip package was found to seal well and hold the liquid sample during thermal testing.

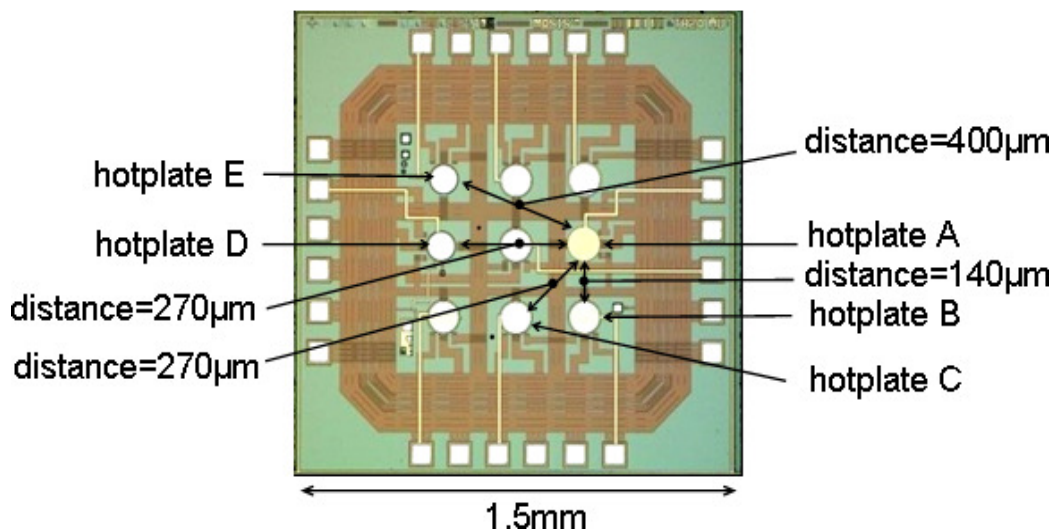


Figure 3. 4. Die photograph of the 1.5x1.5mm microhotplate 3x3 array.

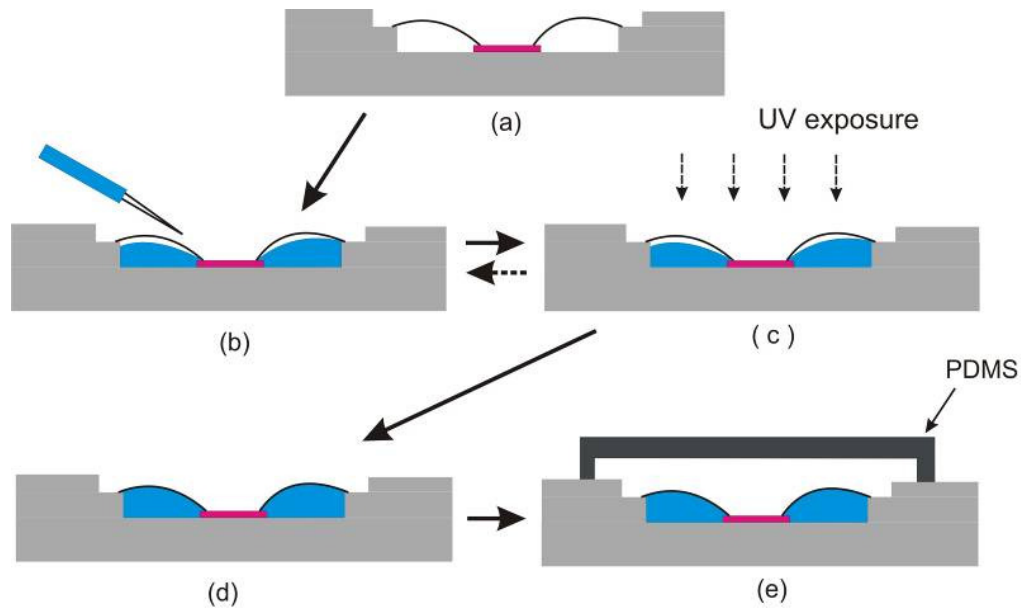


Figure 3.5. Chip packaging flow: (a) chip in DIP40; (b) dispense SU8 2002 using a syringe; (c) soft baking, UV exposure and hard baking; (d) final SU8 reservoir; (e) PDMS cap on DIP40 package. Steps (b) and (c) are repeated 4 or 5 times until package is fully filled with SU8.

3.3 Measurement Results and Analysis

A test board was developed to connect the thermal control array chip to a PC equipped with a data acquisition card, and a LabVIEW[®] program was designed to track and record the sensor temperature. The chip was first placed in an environmental test chamber to determine the poly1 sensor resistor's temperature coefficient of resistance (TCR). The poly1 resistance was found to decrease linearly with temperature from 27-80°C, and a TCR of -1, 520 ~ -3, 220ppm/°C was calculated, with similar results for all sensor

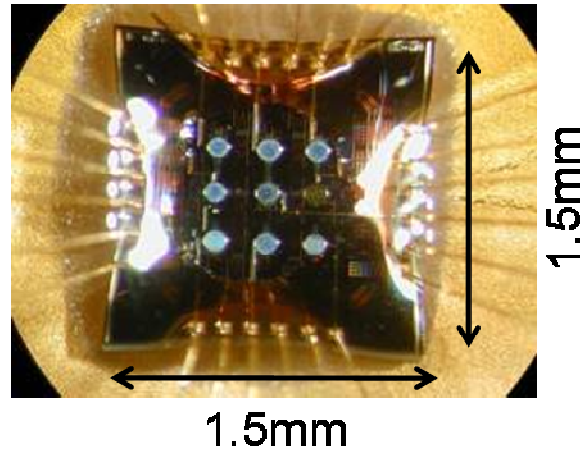


Figure 3. 6. The 1.5x1.5mm wire bonded first thermal CMOS chip encapsulated with SU8 2002. There are 3x3 microhotplate array in the chip.

resistors on the chip. To improve the measurement precision, it is better to calibrate the TCR in every chip fabrication because TCR is sensitive to the process.

After calibrating the PID controller, a step response test of the entire thermal control system was performed at room temperature by setting the desired temperature from 27 to 42°C in 3 °C steps. The temperature was held constant for 60 seconds before each step. The results plotted in Figure 3.7 show that the thermal settling time increases with temperature, as expected, with about 14 seconds to step to 30°C. Once the set point is reached, the temperature is held very stable by the feedback controller; extensive testing shows a maximum error of only 0.7 °C over the entire span of operation.

The heating potential of the on-chip microhotplate as a function of heater voltage was tested in both air and liquid environments. The results in Figure 3.8 show that, as expected, higher voltages generate higher maximum temperatures. Although the maximum temperature is slightly higher in air, the microhotplate in liquid was able to rise to nearly 45 °C with only a 5 V heater drive voltage. Because the heater drive voltage connects only to the heater resistor and not to CMOS devices, a higher voltage could be used to increase the temperature. However, 45 °C is sufficient to characterize most proteins or to maximize their reactivity for sensor applications. For example, our colleagues in Dr. R. Mark Worden’s lab have characterized the temperature dependence of NEST (NEST is a hydrophobic recombinant polypeptide comprising the catalytic domain (residues 727–1216) of neuropathy target esterase [51]), a catalytically active fragment of the membrane protein Neuropathy Target Esterase (NTE) found in human neurons. Figure 3.9 plots the NEST thermal characteristics in the range of 20 °C – 60 °C,

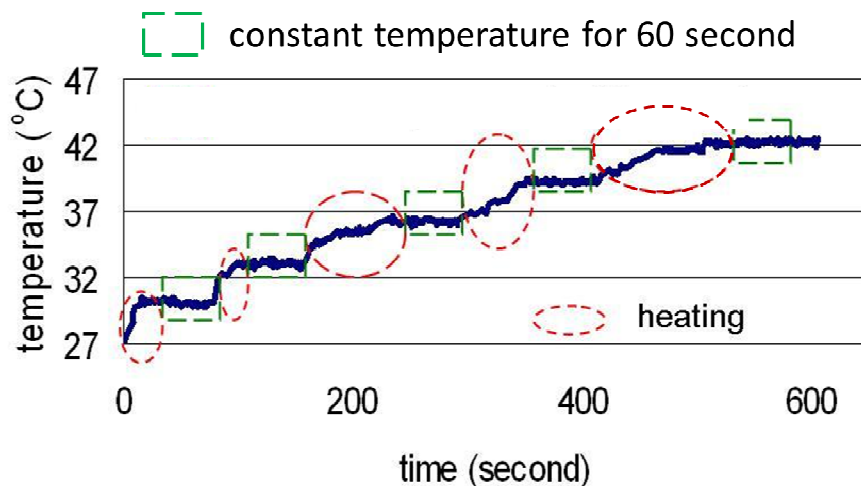


Figure 3.7. Thermal step response of the microhotplate thermal control system for 3 °C steps.

showing a typical parabolic function with maximum activity at 31 °C after which activity irreversibly degrades. The microhotplate array microsystem is well suited to thermally control this and similar proteins.

Finite element analysis simulations predicted that the heat from of each array element would be contained in very close proximity to the heating element, even without additional processing steps to improve the thermal isolation of each heater. This self-contained heading would permit each array element to be set to a different temperature for simultaneous characterization at multiple temperatures. To test this prediction, an experiment was conducted where one array element was heated and the temperature sensors of several other array elements were monitored. Referring to labels in Figure 3.4, a 5 V source was applied to the heater in array element ‘A’ for more than 10 min to ensure the maximum temperature was reached. Microhotplate temperature sensor values at elements ‘A’ – ‘E’ were then recorded. Figure 3.10 plots the results as a function of the

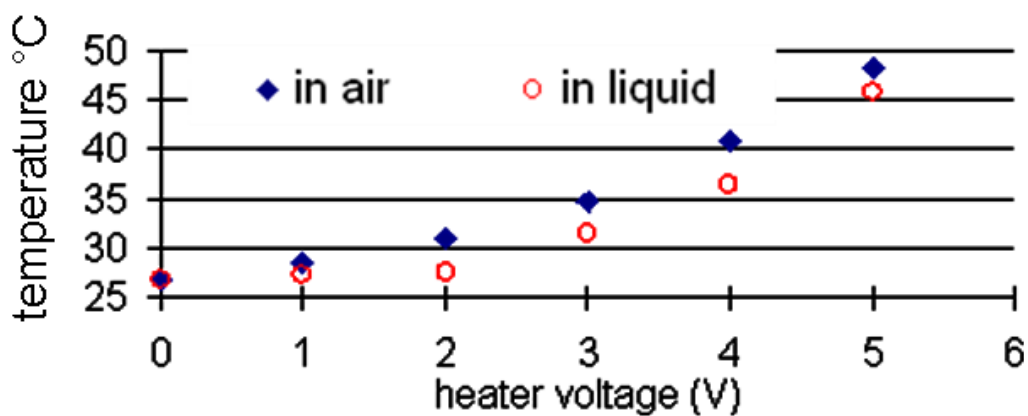


Figure 3.8. Temperature (at on-chip sensor) in air and in liquid at different heater voltages.

sensor's distance from the one active heater, 'A'. As expected, as distance increases the thermal isolation improves, and at only 0.4mm from the heater the induced temperature change is less than 1 °C. Although the thermal isolation was not as strong as predicted by simulations, these results verify that it is feasible to simultaneously set individual elements of the array to different temperatures. Even on the tiny 1.5×1.5 mm chip tested here, a highly isolated 2×2 array could easily be formed.

3.4 Summary and Analysis

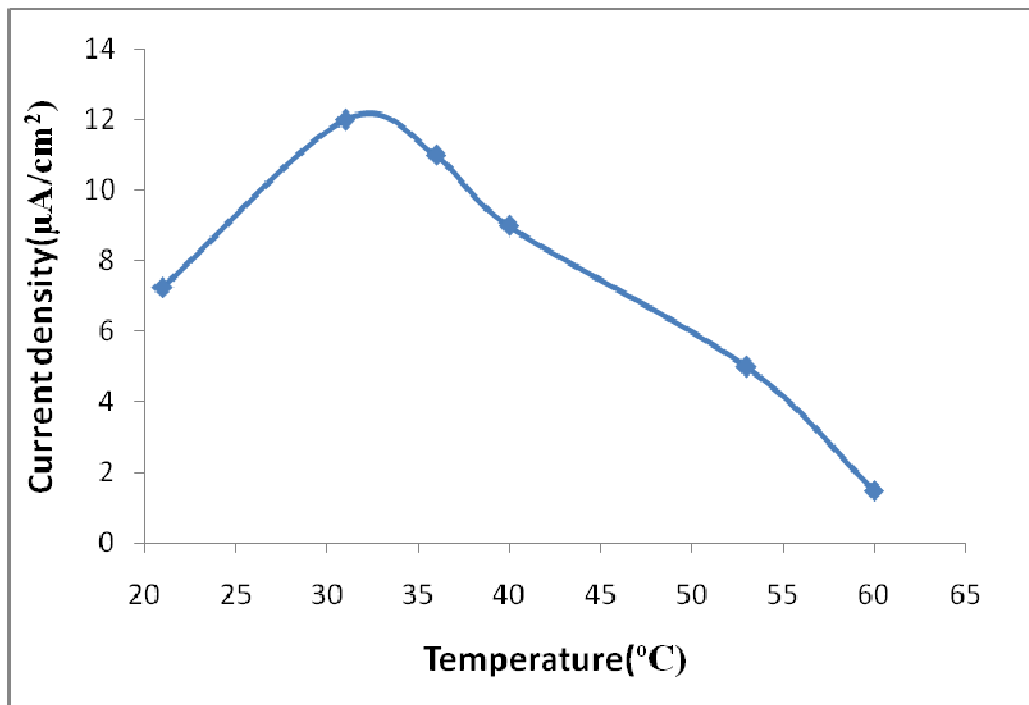


Figure 3.9. Current density of a NEST (NEST is a hydrophobic recombinant polypeptide comprising the catalytic domain (residues 727–1216) of neuropathy target esterase) biosensor at different temperatures.

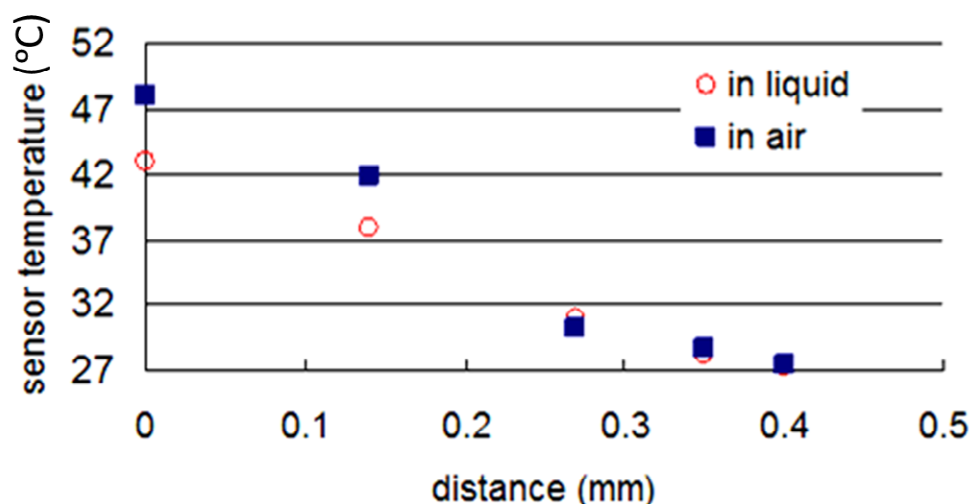


Figure 3.10. The sensor measured temperature vs. the distance from the heating source to the sensor.

A complete thermal control microsystem for protein characterization and sensing was developed and tested. The CMOS hotplate design ensures good spatial uniformity with no local hotspots. The chip was fabricated in a standard CMOS process and packaged using layering of SU8 for use in a liquid environment. A maximum temperature of 45 °C was achieved in liquid with a 5V supply. The thermal control microsystem can set and hold temperatures within 0.7 °C, and array elements were found to be almost completely thermally isolated from each other at distances beyond 0.4 mm.

These test results proved our designed thermal microsystem is suitable for the protein characterization. However, the thermal controller was implemented using an off-chip PID controller, the chip did not include a sensor to monitor the ambient temperature, and the chip did not include any readout circuits. To achieve a fully integrated protein thermal control system, these elements are very important. Building on the efforts described in this

chapter, the second generation thermal controlled protein characterization chip, introduced at Chapter 5, implements these improvements

Chapter 4

Impedance Extraction Circuits for Protein Array

Traditionally, impedance spectroscopy measurements require complex and bulky electronics or utilize digital signal processing algorithms that require extensive computer hardware. To support chip-scale microsystem applications, a very hardware efficient and low power solution is needed that combines accurate, low noise impedance measurement circuits with electronics capable of extracting real and imaginary signal components and circumvents the heavy signal processing load incurred by parallel impedance extraction of a sensor array [52, 53]. Some impedance measurement systems have been built for miniaturized biomedical and biochemical systems [53-55], but they either lack the integration of measurement, extraction, and digitization functions or they fail to support multi-channel array-based systems.

In this chapter, a compact, high-sensitivity lock-in impedance-to-digital converter (IDC) circuit for sensor array microsystems is presented. The lock-in IDC cell is based on a delta-sigma structure and can be instantiated for each sensor element to enable massively parallel interrogation, including analog domain impedance extraction and local digitization. Its low power consumption extends the battery-life for portable applications and protects on-chip sensors from overheating. It also provides high sensitivity to read

the very weak responses characteristic of miniaturized sensor elements. Compared to prior works in our lab [56], the new impedance measurement circuit presented here adds DC impedance readout capability and implements design modifications that reduce power and area, thus improving the utility of the circuit in array-based microsystems.

4.1 Architecture of Impedance Extraction

Circuits

There are three main concerns for integrating on a single chip all of the instrumentation functions for multi-channel impedance extraction. First, the heavy signal processing load must be simplified, which is especially true for multi-channel arrays. Second, the circuit area per channel must be minimized to maximize the potential array density in support of high throughput characterization goals. Finally, the power must be minimized to support portable applications and ensure no local heating that could degrade on-chip biointerfaces. To support these goals, an impedance extraction front-end instrumentation circuit based on the frequency response analyzer (FRA) method was developed. The FRA method processes the response of one frequency point at a time. It is a pure technique that gives rise to very stable, repeatable measurements, can be realized with compact analog circuits, and is able to minimize the effects of noise and distortion. Moreover, if all of the analog circuits can operate in the weak inversion region, static power consumption can be minimized and noise performance can be improved.

4.2 Impedance Readout Circuit

The IS measurement circuit presented here is based on a delta-sigma structure and will be referred to as the lock-in IDC, as defined in prior work in our lab [53]. Utilizing the FRA method, the lock-in IDC scheme simultaneously computes and digitizes the real or imaginary response components, sharing hardware required for these operations to minimize the power and area of the circuit.

4.2.1 Theory of Operation

The derivation of lock-in IDC operation was reported in [53] and was repeated here for clarity. To describe FRA method and the operation of the lock-in IDC, consider a sensor interface stimulated by a sinusoidal voltage, $\sin(\omega t)$, and producing a current response I_X such that

$$I_X = A \sin(\omega t + \theta) = a \sin(\omega t) + b \cos(\omega t) \quad (4-1)$$

where A and θ represent the amplitude and phase, of the sensor's impedance, respectively. Here $a = A \cos(\theta)$ is the *real* portion and $b = A \sin(\theta)$ is the *imaginary* portion of the sensor's admittance (the reciprocal of impedance). The values of a and b over a wide frequency range are sufficient to fully describe the sensor's impedance response.

To extract the values of a and b , a multiplying integrator was designed for the lock-in IDC. As shown in Figure 4.1, the multiplier is driven by a square wave, $\varphi(t)$. When control signal S in Figure 4.1 is set to 0, $\varphi(t)$ is in phase with $\sin(\omega t)$ and is described by

$$\phi(t) = \text{sgn}(\sin(\omega t)) = \begin{cases} 1, & nT \leq t < nT + T/2 \\ -1, & nT + T/2 \leq t < (n+1)T \end{cases} \quad (4-2)$$

where T is the period of the stimulus and n is any integer. If (4-1) is multiplied by (4-2) and integrated over N continuous stimulus cycles, then the integrator's output is given by

$$\begin{aligned} \int_0^{NT} I_x \cdot \phi dt &= \sum_{i=0}^{N-1} \left(\int_{iT}^{(i+1/2)T} I_x dt - \int_{(i+1/2)T}^{(i+1)T} I_x dt \right) \\ &= \frac{2T}{\pi} \cdot N \cdot A \cos(\theta) \end{aligned} \quad (4-3)$$

Notice that the integration result is proportional to the *real* portion of the sensor's

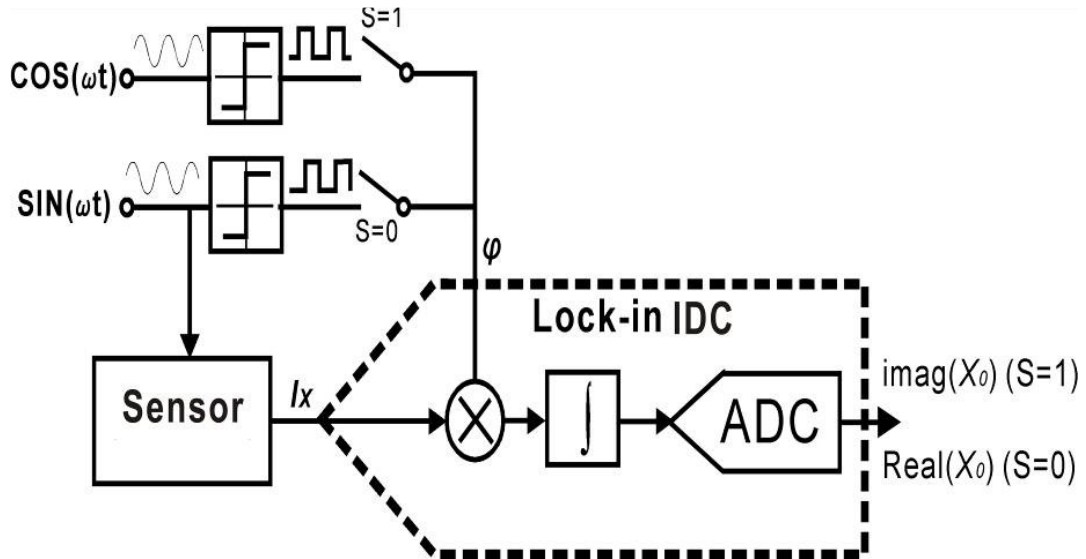


Figure 4.1. IDC functional blocks derived from the FRA method. The circuit extracts the *imaginary* portion of admittance when $S=1$ and *real* portion when $S=0$.

admittance, a in (4-1). Similarly, if the square wave $\phi(t)$ is in phase with $\cos(\omega t)$ (when $S=1$), its function is given by

$$\phi(t) = \text{sgn}(\cos(\omega t)) = \begin{cases} -1, & nT + T/4 \leq t < (nT + 4T/3) \\ 1, & \text{else} \end{cases} \quad (4-4)$$

and the result of the operations in (4-3) give

$$\int_0^{NT} I_x \cdot \phi dt = \frac{2T}{\pi} \cdot N \cdot A \sin(\theta) \quad (4-5)$$

which shows that the result is proportional to the *imaginary* portion of the sensor's admittance, b in (4-1). Thus, with a multiplier, an integrator, and two reference square-waves, the impedance extraction function can be realized in hardware.

4.2.2 IDC Circuit Implementation

To implement the FRA functionality described above while also digitizing the resulting admittance value, the lock-in IDC structure shown in Figure 4.2 was developed. It includes an analog multiplying integrator stage to realize impedance extraction via the FRA method, and a comparator, a flip-flop, and a bidirectional counter for digitization. Without the switches controlled by ϕ , the structure is similar to a traditional delta-sigma ADC, where the comparator is a 1-bit ADC and the reference currents are a 1-bit DAC. This structure was selected as the foundation for the IDC because it both includes the integrating function required for impedance extraction and also permits sufficient accuracy in a compact size with no external components required.

The first stage of the lock-in IDC is a multiplying integrator stage that is based on previous work in our lab [56]. It shares resources to realize both the multiplication and integration functions shown in Figure 4-1. The multiplying integrator changes its polarity according to the value of the square wave ϕ .

To simplify analysis, assume 1) that ϕ is in phase with $\sin(\omega t)$ and 2) that at all of ϕ 's transition edges both comparator results, D and D*, are low. If not, the multiplexing switches controlled by ϕ force D and D* to exchange the polarity of charge injection through reference current I_{ref1} or I_{ref2} . From time 0 to T/2, ϕ is high and the counter in Figure 4.2 is counting up. Just before ϕ 's edge at time T/2, according to the charge conservation theory, at the input node, we have

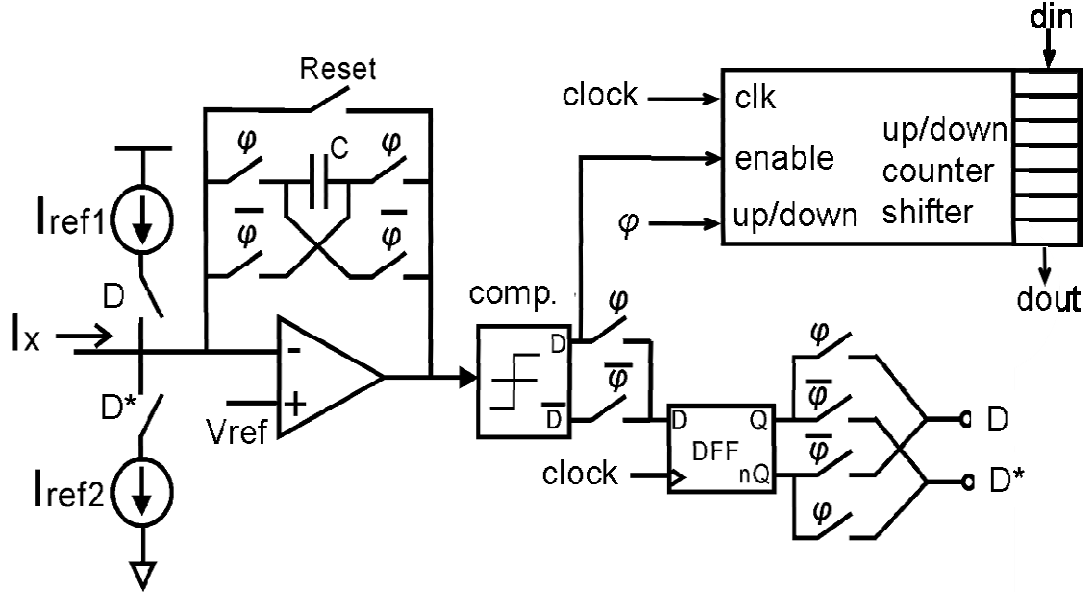


Figure 4.2. Simplified lock-in impedance-to-digital converter structure. ϕ is the reference square wave.

$$\int_0^{T/2} I_x \cdot dt = CV_{res1} + I_{ref1} T_0 \sum_{i=1}^N D_i - I_{ref2} T_0 \sum_{i=1}^N D_i^* \quad (4-6)$$

where V_{res1} is the residue value at the integrator output, T_0 is the updating clock period, and N is the number of clock cycles from time 0 to $T/2$. From time $T/2$ to T , ϕ is low, the integrator capacitor is reversed, and the counter is set to down counting mode. This mode produces

$$\int_{T/2}^T I_x \cdot dt = C(V_{res1} + V_{res2}) + I_{ref1} T_0 \sum_{i=N+1}^{2N} D_i - I_{ref2} T_0 \sum_{i=N+1}^{2N} D_i^* \quad (4-7)$$

where V_{res2} is the integrator's output voltage at time T . Simplifying the equation with $D^*=1-D$ and combining (4-6) and (4-7), the full cycle produces

$$\int_0^T I_X dt = -CV_{res2} + (I_{ref1} + I_{ref2}) \cdot T_0 \left(\sum_1^N D_i - \sum_{N+1}^{2N} D_i \right) \quad (4-8)$$

Thus, the *real* result is represented by the contents of the counter (the summations in (4-8)), provided the circuit parameters are chosen such that

$$|CV_{res2}| < \frac{1}{2} \min(I_{ref1} T_0, I_{ref2} T_0) ,$$

where the residue on the integrator can be

treated as noise. If the IDC is operated for N consecutive stimulus cycles after initial reset, the residue term in (4-8) remains in the same range while the digital part is magnified by N . Therefore, the error due to ignoring the residual will decrease with repeated cycles.

Following a similar analysis, it can be shown that the counter will contain the *imaginary* portion of admittance when φ is in phase with $\cos(\omega t)$. The *imaginary* portion can be presented by

$$\begin{aligned} \text{imaginary portion} &= \frac{\pi}{2TN} \cdot \int_0^{NT} I_{in}(t) \cdot \varphi(t) dt \\ &= \frac{\pi T_0}{2T} \cdot (I_{ref1} + I_{ref2}) \cdot \left(\sum_{N/4}^{3N/4} D_i - \sum_1^{N/4} D_i - \sum_{3N/4+1}^N D_i \right) \end{aligned} \quad (4-9)$$

Thus, by setting ϕ to be in or out of phase with the stimulus sinusoid, the IDC circuit can extract both portions of the full impedance utilizing a structure that inherently digitizes the result while sharing resources to minimize size and power. The bidirectional counter also serves as a shift register to permit serial data upload of all channels.

Compared to [53], the new circuit presented here only includes one comparator, and one bidirectional counter for digitization instead of two. This compact structure IDC saved 25% area comparing with [53] and maintains same performance. Further, this IDC circuit has DC impedance readout capability as sigma-delta ADC, when keep ϕ in a certain status (turn on/off).

Chapter 5

Second Generation Thermal

Control Chip with Test Results

5.1 Second Generation Thermal Control Chip

Design

Measurement results reported in Chapter 3 proved the thermal microsystem method is suitable for the protein sensing. However, the thermal controllers presented in Chapter 3 are off chip. Furthermore, the first generation thermal control chip presented in Chapter 3 did not include an ambient temperature monitor or any sensor readout circuits, which are both important to the complete microsystem implementation. To achieve a fully integrated protein thermal control on-chip instrument, all these elements should be in a single chip. A hardware efficient and integrated second generation thermal control chip, which includes on-chip thermal controller, ambient temperature sensor and protein characterization circuits, was developed in 0.5 μ m CMOS process. The concept of the thermal system is shown in Figure 5.1, where the thermal control circuits set the temperature of each protein site separately and the readout circuits (IDC, reported in Chapter 4) detect the protein reaction signals through the working electrode (WE) at the temperature of the maximum

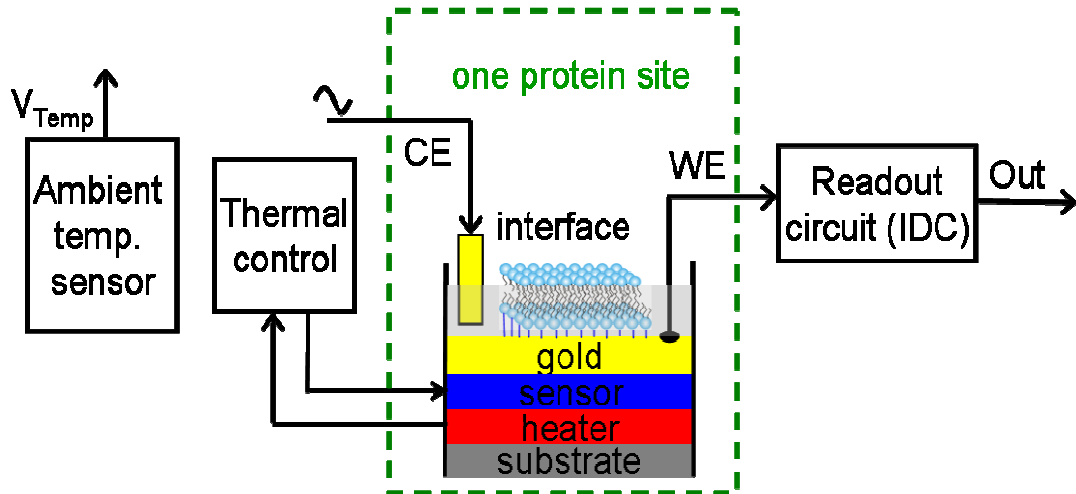


Figure 5. 1. The concept of the second generation thermal control chip. The ambient temperature sensor block detects the temperature of whole chip. Thermal control block controls the temperature of each protein site locally. The IDC circuit characterizes the activity of the protein interface.

activity of the proteins. Additionally, the ambient temperature sensor monitors the temperature away from the heater sites.

5.1.1 Ambient Temperature Sensor Design

In the heating process, it is important to track the ambient chip temperature and then make sure the protein sites are heated locally without heating the entire chip. Furthermore, it was desired to enable a “cold sensing” measurement scheme where the sample remains cold, to extend its lifetime, and is only heated at the local protein sites. To monitor the temperature of the whole chip, an ambient temperature sensor was designed based on the well-known CMOS proportional to absolute temperature (PTAT) technique [57], which is based on the drain current, I_D , being proportion to the ambient temperature when the transistor is working in weak inversion region:

$$I_D = I_{D0} e^{\frac{V_{GS} - V_{th}}{nV_T}} \quad (5-1)$$

where I_{D0} is a process-dependent parameter, n is the slope factor, $V_T = kT/q$ is thermal voltage.

The designed PTAT ambient temperature sensing circuit is shown in Figure 5.2, where M5, M6 operated in weak inversion region. According to (5-1), current I_1 and I_2 are exponentially related to the ambient temperature T . I_2 is copied to I_3 by current mirror M4, M7 and these currents run through resistors R_1 and R_2 , the output voltage, V_{amb_temp} , which is proportional to absolute temperature T , and can be expressed as following,

$$V_{amb_temp} = V_T \cdot \frac{R_2}{R_1} \ln \left(\frac{\left(\frac{W}{L}\right)_5}{\left(\frac{W}{L}\right)_6} \right) = \left[\frac{k}{q} \cdot \frac{R_2}{R_1} \cdot \ln \left(\frac{\left(\frac{W}{L}\right)_5}{\left(\frac{W}{L}\right)_6} \right) \right] \cdot T \quad (5-2)$$

The start-up circuit, M1-M2, provides an initial transient current into the drain of M5 during power-up. This causes the PTAT ambient temperature sensor to settle in the correct state and to be self-biasing.

5.1.2 Thermal Controller Circuit Design

In designing the thermal controller for the second generation thermal control chip, it is important to consider the hardware efficiency of the thermal controller circuit. For example, in a 1.5x1.5mm chip, more than half of the area would be occupied by the protein array and microhotplates and not available for circuitry including the controller and the readout circuits. This area is required because the membrane protein interfaces need to be at least 100 μm in diameter to avoid the edge effect, which were observed to affect the performance and function of the membrane proteins when the interface sizes were too small. Another reason is that the P/N MOS power transistors used to drive the

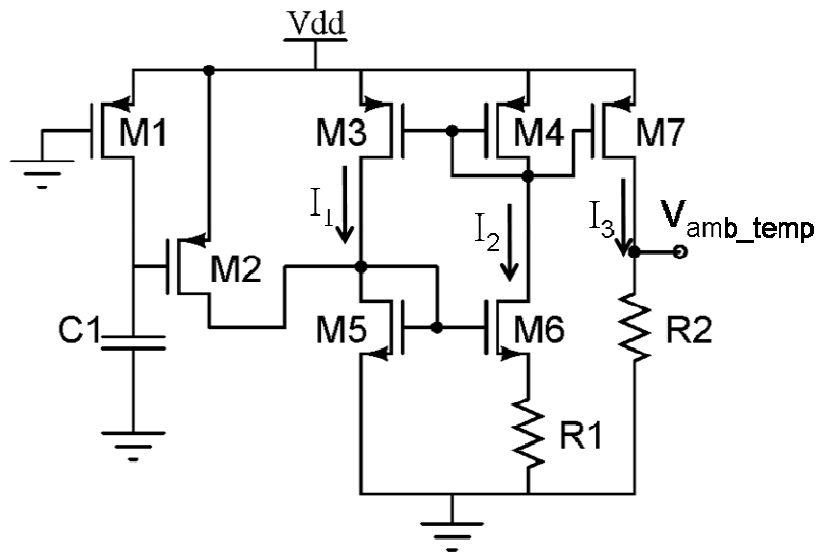


Figure 5.2. The simplified schematic of the CMOS PTAT ambient temperature sensing circuit.

heaters also occupy a large area. In [58], the switch transistor size was set to $W/L=1500\mu\text{m}/0.8\mu\text{m}$ to ensure sufficient current without damaging the switch. In our design, $W/L=800\mu\text{m}/0.8\mu\text{m}$ was chosen according to calculations of the possible maximum current through these switches at 5V supply voltage. Furthermore, to achieve thermal isolation, the distance between microhotplates should be larger than $400\mu\text{m}$ based on the test results in Chapter 3.

An analog thermal controller was selected for the second generation thermal control chip because it is more hardware efficient than a digital thermal controller. The designed analog thermal controller is shown in Figure 5.3. The operation of the analog thermal controller is that the comparator compares the desired setpoint voltage (V_{set}) with the temperature sensor (R_S) feedback voltage (V_{fb}). The power transistor (switch) turns on/off the current through the heater (R_H) based on the output of comparator. To increase the sensitivity of the thermal controller, the temperature sensor output voltage was

amplified by gain $-\frac{R_f}{R_1}$, where R_f is a programmable variable resistor. Furthermore,

to improve the system stability and reduce noise, a hysteresis comparator was used to separate the up-going and down-going switching points so that, once a transition has started, the input must undergo a significant reversal before the reverse transition can occur. If only one signal switching point were used in the comparator, any noise at the input of the comparator would be amplified and cause the output of comparator to bounce back and forth. This is unacceptable in most applications, but it can generally be cured by introducing hysteresis.

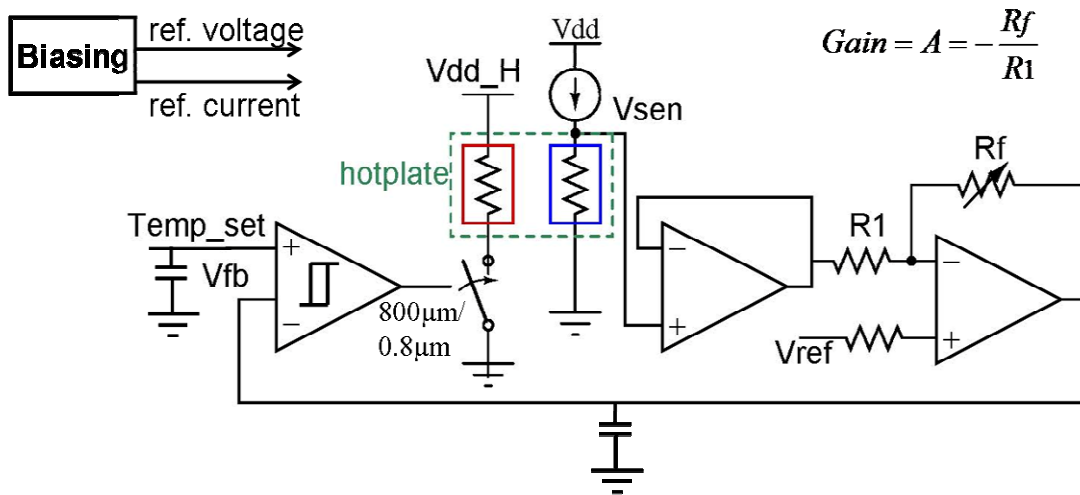


Figure 5.3. The schematic of second generation thermal controller. The comparator used to control switched is a hysteresis comparator to reduce thermal noise.

The schematic of amplifier used in the thermal controller is shown in Figure 5.4. A Miller capacitor structure was used to support enough phase margins for system stability. The amplifier was designed to achieve 100 dB DC gain, 74° phase margin and 1.62 kHz bandwidth.

In the thermal control chip, the comparators, amplifiers, and current mirrors need temperature independent voltage and current references to maintain constant performance over a wide temperature range. To generate on-chip temperature independent reference voltage and current, a biasing circuit was developed based on [59]. The benefit of this structure is allows both strong supply scaling and all-MOS implementation by the use of MOS subthreshold techniques in the Log domain[59]. The concept of this references generator was using a feedback loop (P) to cancel the PTAT voltage gain (1/G) to achieve a temperature independent reference voltage V_{ref} by setting set $P/G=1$. The current reference I_{ref} can be easily generated by V_{ref} through a transconductance (Z) circuit.

The schematic of the reference circuit was shown in Figure 5.5 (b), where M1-M2 operates as a start up circuit, and M6, M7 are PTAT voltage core with operating in weak inversion region. As explained in the previous section, for a PTAT voltage, the reference voltage exhibits

$$V_{ref} = V_T \ln(G) \quad (5-3)$$

where $G = I_2/I_1$. According to the feedback loop requirements, $P/G=1$, (5-3) can be rewritten as

$$V_{ref} = V_T \ln(P) \quad (5-4)$$

The feedback loop gain, P can be obtained through geometry scaling, such as current mirror. In this circuit, the gain was achieved by setting the size of transistor M13 is P

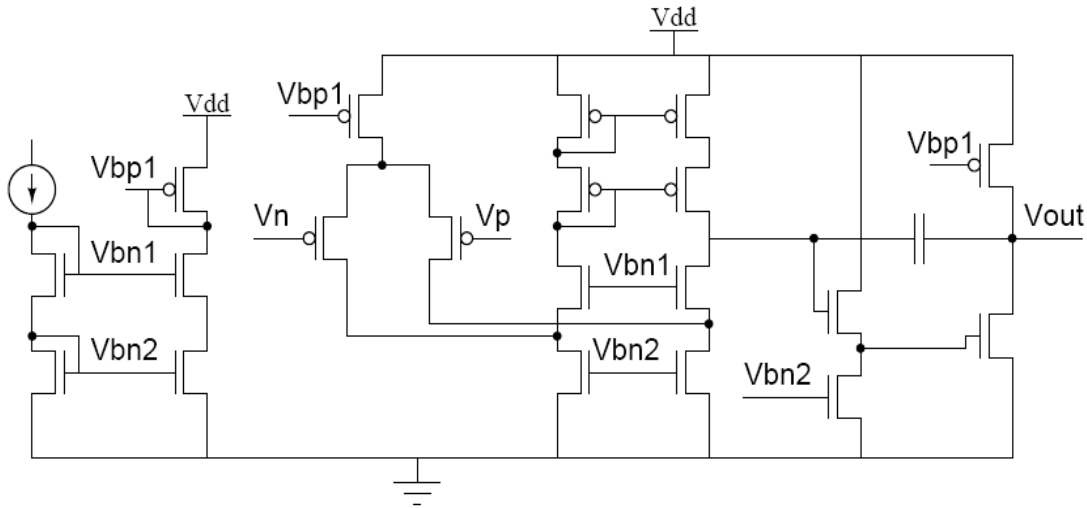


Figure 5.4. The schematic of the amplifier used in the thermal controller.

$$\frac{\Delta V_{ref}}{V_{ref}} = \frac{\ln(1 + \frac{\Delta P}{P})}{\ln(P)} \approx \frac{1}{\ln P} (\frac{\Delta P}{P}), \text{ here } \Delta P \ll P \quad (5-5)$$

Due to the log dependence on factor P , the maximum V_{ref} variance is located at small P , such as $P \rightarrow 1$, while V_{ref} robustness increases for $P \rightarrow \infty$. Hence, high-sensitivity regions could be avoided by larger factor P . In our design, $P=20$ was selected as the trade off between resolution and size. Moreover, ΔP is typically associated to technology mismatching at transistor level, so good matching technique must be taken into account during design stage.

From V_{ref} , it is easy to generate reference current I_{ref} by a voltage to current convertor. Furthermore, C1, C2 were used to make sure the system stable and reduce noise.

5.2 Test Results

The second generation thermal control chip was fabricated in 0.5 μm CMOS process, and the die photograph is shown in Figure 5.6. Two microhotplates with 100 μm and 200 μm diameter, two thermal controllers and two- IDC readout channels were integrated on a 1.5mm x 1.5 mm chip. To characterize the performance of the two functional circuit blocks, the thermal controller and the IDC readout blocks were tested separately.

5.2.1 Thermal Control Circuit Test Results

To measure the accuracy of the temperature independent reference voltage and current generator, the thermal control chip was placed in a programmable temperature oven (AH-202XS) that can be controlled by a computer through RS232/GPIB protocol. The output reference voltage and current signals from the biasing circuit were record by a data acquisition card (Agilent, 6259). The measured results of voltage and current reference from 10 to 70 °C are shown in Figure 5.7. The temperature variation of the voltage reference and the current reference is less than 0.04% and 0.3%, respectively.

To measure the analog thermal controller performance, a linearity response test of the entire thermal control circuit was performed in air by setting the desired temperature to 50 °C from a room temperature (25 °C) starting point. The results plotted in Figure 5.8 showed that the temperature was held stable by the feedback controller with a maximum

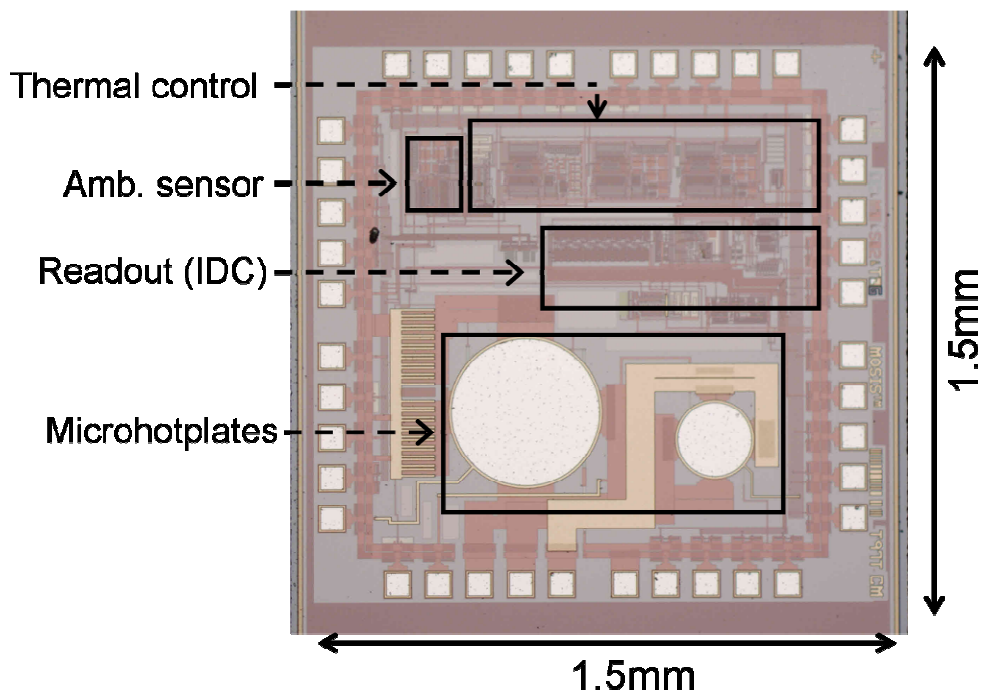
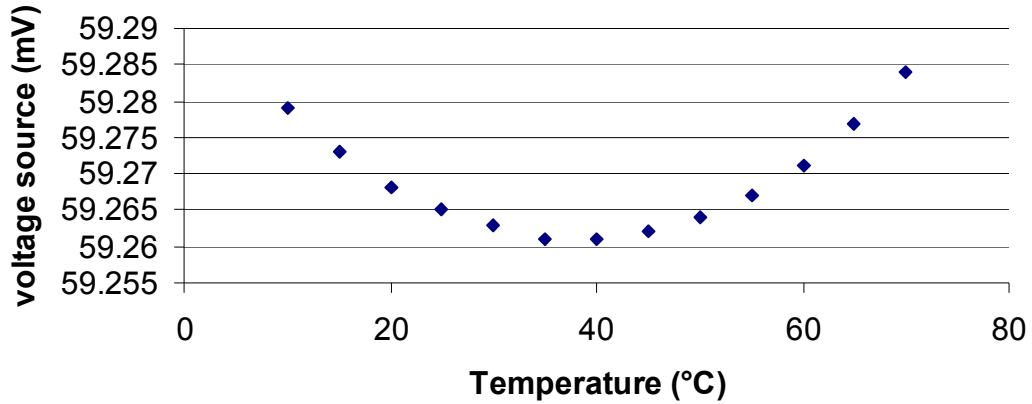
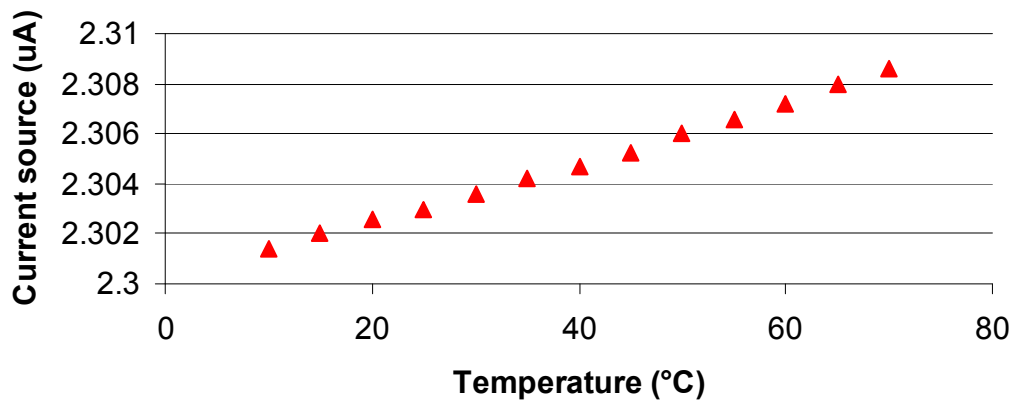


Figure 5.6. Die photograph of second generation thermal control chip.



(a) Test results of voltage source at different temperature.



(b) Test results of current source at different temperature.

Figure 5.7. The test result of voltage (a) and current (b) reference with temperature for 10°C to 70 °C.

error of ± 1 °C over the entire span of operation when the set point was reached. This temperature resolution can meet the proteins test requirements [55].

5.2.2 IDC Circuit Test Results

5.2.2.1 Circuit Characterization

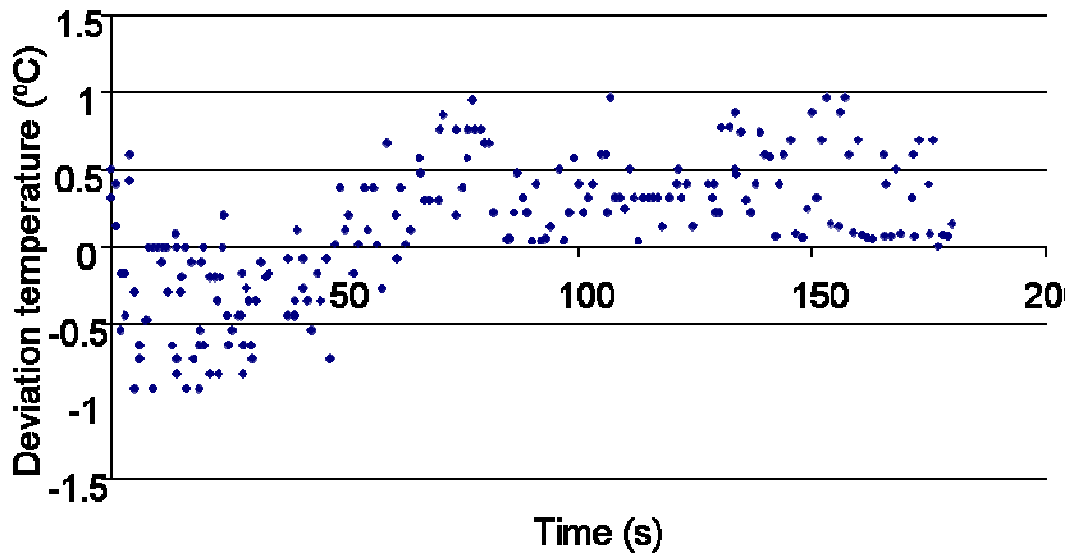


Figure 5.8. The deviation between set point temperature (Temp_set) and measured temperature for 25 °C to 50 °C with gain=2 setting measured 180 second.

To test the performance of the IDC circuit, a data acquisition card (DAQ 6259) was used to generate the sinusoid stimulus voltage, reference square wave, global clock and digital control signals and to record digital output results from the lock-in IDC on the second generation thermal control chip. An equivalent impedance model for a biomimetic membrane sensor interface [60] was utilized to characterize the chip. This model is shown in Figure 5.9 along with other elements of the IDC test setup.

To verify the impedance extraction capability of the lock-in IDC circuit, a sinusoidal voltage stimulus with frequency from 0.1 to 100Hz was applied to the biosensor circuit model. Figure 5.9 plots the results obtained from the digital output of the IDC along with the theoretical curve for the model impedance. The lock-in IDC tracks both *real* and *imaginary* components of the test impedance very well, with a maximum mismatch of 1% of the full scale response.

Figure 5.10 demonstrates that the IDC tracks static impedance over frequency very well. To characterize the circuit's response to variable impedance, an IDC channel output was recorded while independently changing the phase and amplitude of the stimulus input. Ideally, the relationship between the input signal's amplitude and the digitized *real* component output is linear for a constant phase and frequency. To verify the amplitude transfer function, a 10Hz, zero initial phase sinusoid signal with amplitude swept from 0 to 10nA was supplied. The measured differential nonlinear (DNL) and integral non-linear (INL) of the digitized *real* portion output are plotted in the Figure 5.11, which shows that the *real* portion dynamic range is more than 50.2 dB for the 10nA input range.

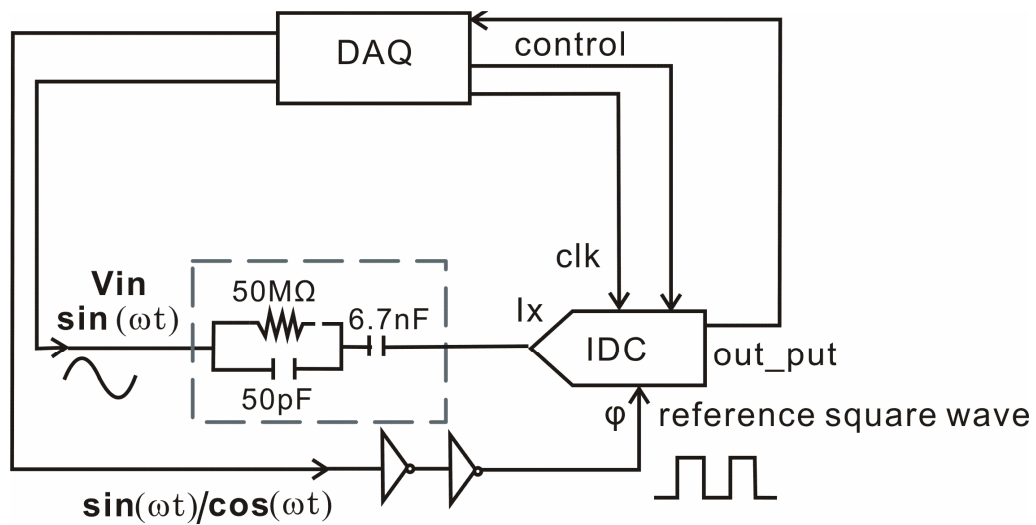


Figure. 5. 9. Test platform for the IDC chip with biosensor equivalent circuit model.

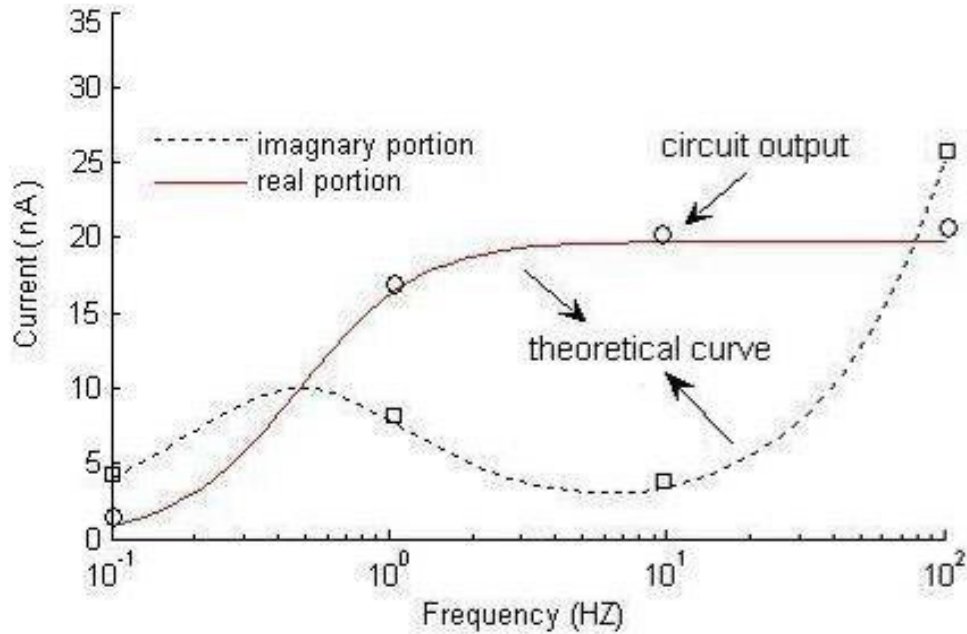


Figure 5.10. The real (circles) and imaginary (squares) results from the IDC circuit for the test setup shown in Figure 5.9 along with theoretical (expected) curve for comparison.

The relationship between the input signal's phase and the digitized *imaginary* component output is theoretically a sine wave for a constant amplitude and frequency. To measure the phase transfer function, a cosine input with constant 100Hz frequency, constant 3nA amplitude and variable phase was supplied. The normalized digitized *imaginary* portion output is plotted in Figure 5.12. The output fits the expected sine wave with an RMS error of only 2%.

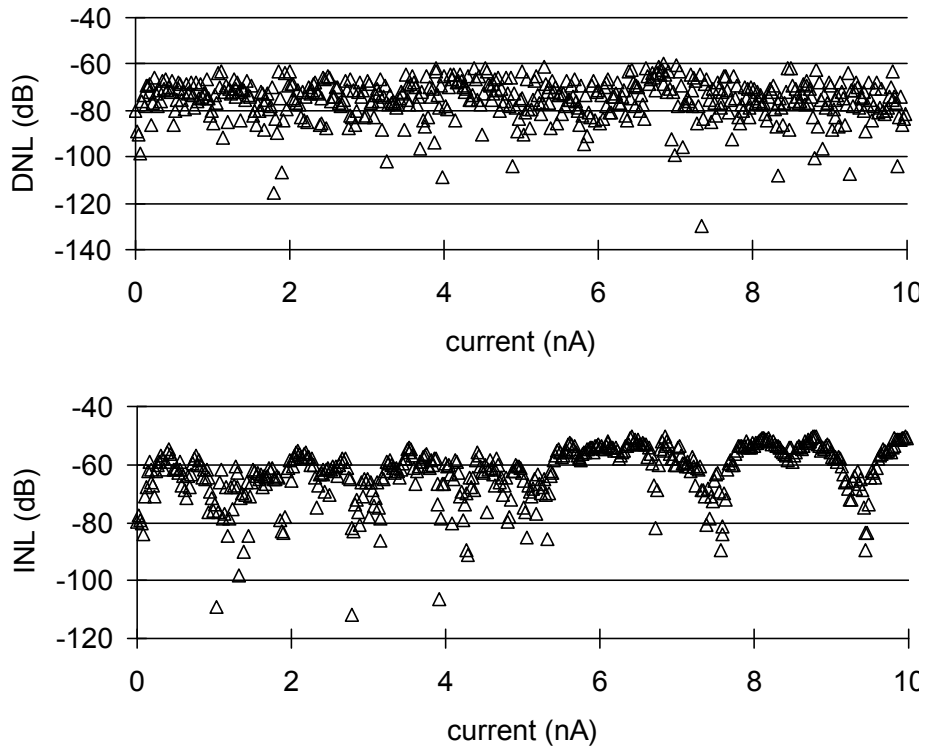


Figure 5.11. Measured DNL and INL curve of one IDC channel output when the sinusoid input amplitude was swept from 0 to 10nA. The maximum DNL and INL are 59.8dB and 50.2dB, respectively.

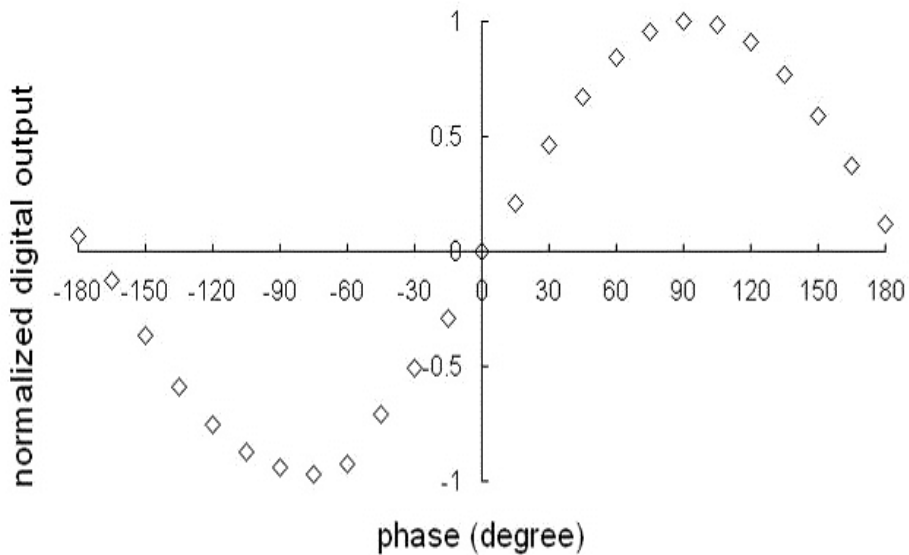


Figure 5.12. Response of an IDC readout channel as the phase of the input signal is varied from -180° to $+180^\circ$ degrees. Input amplitude (30nA) and frequency (100Hz) are kept constant.

The IDC was fabricated in a standard $0.5\mu\text{m}$ CMOS process, and it requires only

0.045mm² per readout channel. The power consumption is 5.2μW per channel with a 3.3V supply and 200 kHz reference clock. The compact size and low power of this circuit enable an IDC cell to be instantiated for every element in a sensor array to increase the interrogation throughput. Around 150 IDC channels can be integrated in a 3x3 mm² chip. Furthermore, the wide dynamic range (0.01-10kHz) and high accuracy of the IDC circuit permit it to support a diverse set of IS-based sensor interfaces. The summary of IDC performance was listed in Table 5-1.

Table 5-1. The performance of impedance-to-digital converter circuit.

Power/channel	5.2 μW@ 3.3V power, f _{clk} =200kHz
Area/channel	0.045 mm ²
Channel density	~150 channels on a 3x3mm chip
Amplitude conversion resolution	7-8 bit
Phase conversion RMS error	<2%
Frequency range	10mHz ~ 10KHz
Maximum input current	100 nA
Maximum current sensitivity	100 fA

5.2.2.2 Biosensor Measurements

To demonstrate the IDC circuit's capabilities in a biosensor system, a hybrid impedance sensor platform described by Figure 5.13 was implemented. A data acquisition card (Agilent 6259) was connected to a computer and employed to generate the stimulus sinusoid and collect output data from the IDC. For the protein interface, a tethered bilayer lipid membrane (tBLM) was deposited on gold electrodes patterned on a silicon chip [61]. First, a self-assembled monolayer (SAM) of 1, 2-dipalmitoyl-*sn*-glycero-3-phosphothioethanol (DPPTE) tether lipid was formed on a clean gold electrode patterned on the silicon chip. Then the upper leaflet of bilayer membrane was deposited by fusion of liposome vesicles made of 1, 2-dioleoyl-*sn*-glycero-3-phosphocholine (DOPC) mobile lipids. Impedance measurements were conducted with the IDC circuit over the frequency range of 10 mHz to 100 Hz while the tBLM was being formed. Figure 5.14 shows the amplitude and phase data obtained from the IDC chip for one electrode as a function of frequency. For comparison, the same biointerface was tested using a commercial electrochemical impedance instrument (CHI 660 B) and those results are included in Figure 5.14. These data showed IDC circuit achieved similar function as

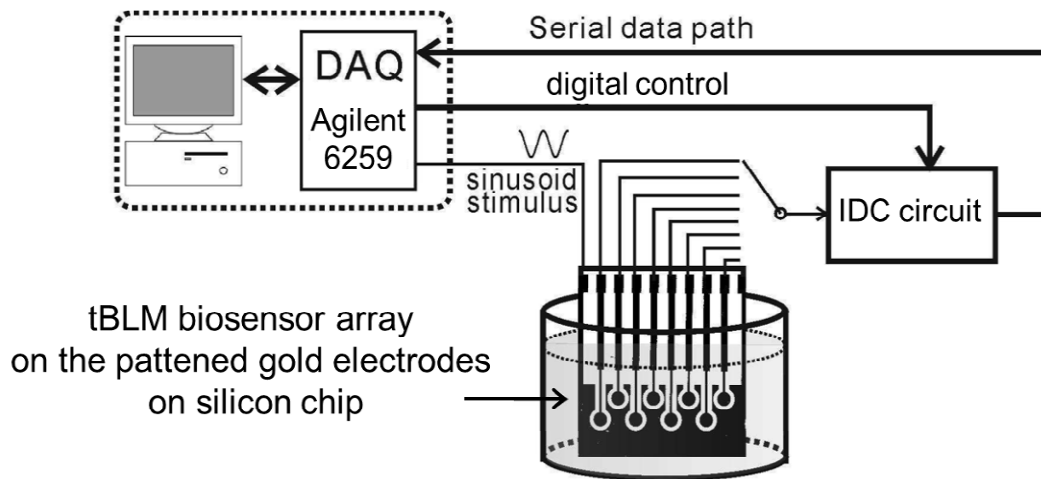


Figure 5.13. The test setup for the biosensor measurements using the IDC circuit.

commercial equipment to extract the impedances of biosensors. The amplitude difference between the commercial instrument and IDC circuit measurement results is less than 0.2% related to the commercial instrument measured impedance data.

To extract the values of each element in the tBLM equivalent circuit model, shown in Figure 2.1, these impedance data measured by IDC circuit was fitted by ZView[®] software. After fitting, the normalized values of each component are $R_s = 95\Omega$, $R_m = 211K\Omega\text{ cm}^2$, $C_m = 0.23\mu\text{F}/\text{cm}^2$, and $C_{dl} = 2.87\mu\text{F}/\text{cm}^2$. These values for tBLM are in good agreement with the reported values for a high quality BLM [62].

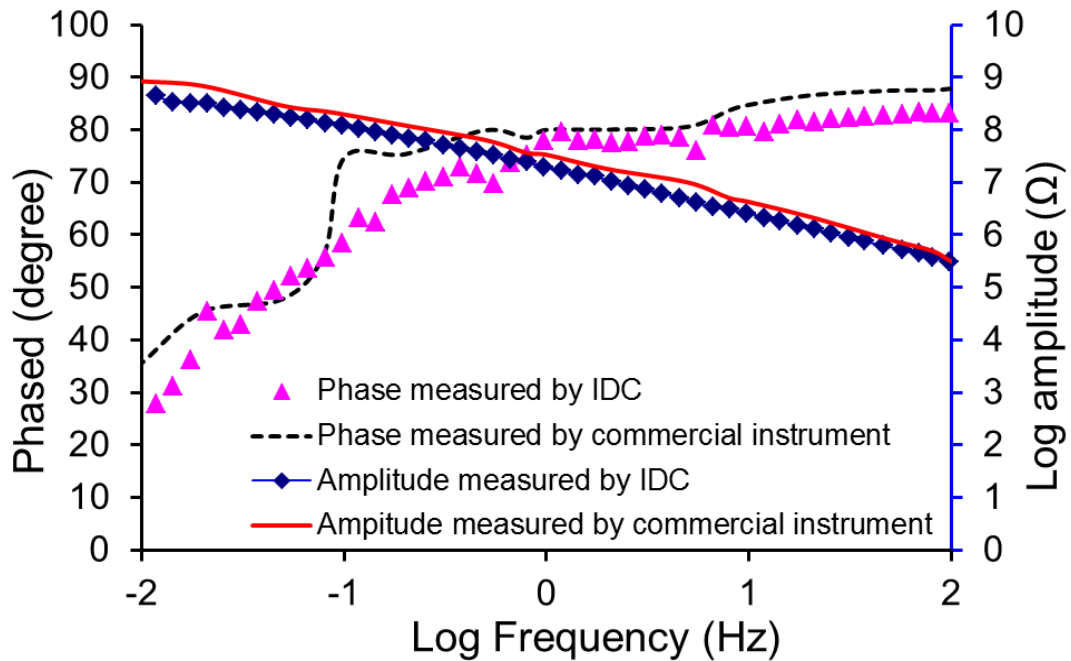


Figure 5.14. tBLM amplitude and phase measured by a commercial instrument (CHI 660 B) and by the fabricated IDC circuit at different frequencies.

Chapter 6

Summary and Future Work

6.1 Summary

In this thesis, a complete thermal control microsystem for protein characterization and sensing was developed and tested. The thermal controllers and microhotplates were demonstrated to heat and hold temperature within ± 1 °C resolution for each protein site. The designed microhotplates are compatible with standard CMOS process and have good spatial uniformity with no local hotspots that could damage a protein interface. A maximum temperature of 45 °C was achieved in liquid with a 5V supply. For the protein characterization, a compact, low power, high-sensitivity lock-in impedance-to-digital converter (IDC) circuit for sensor array microsystem was developed. The IDC circuits locally extracts and digitizes sensor impedance information using mixed-mode signal processing, eliminating the cost, power, and size of the external hardware typically employed to analyze raw sensor data. The IDC readout circuit is extremely hardware efficient, enabling the implementation of a single-chip CMOS microsystem containing an array of microhotplates with individual thermal controllers and readout circuits for each protein sensor site. The main contributions in this research are described below.

A. Developed the first-known CMOS microhotplate array for biosensors in a liquid environment

To our best knowledge, we are the first to report a thermal controlled microsystem suitable for biosensors with CMOS microhotplates without complex silicon etching steps for thermal isolation. Biosensor sites can be heated to individual temperatures, even in a liquid environment. Furthermore, the CMOS hotplate design ensures good spatial uniformity with no local hotspots.

B. Implemented a bioelectrochemical sensor impedance analysis and extraction circuit with the highest density (channels/area) reported.

The developed impedance-to-digital converter (IDC) extracts real and imaginary impedance components and digitizes results without any external hardware. Its area is only 0.045mm^2 per readout channel in a standard $0.5\mu\text{m}$ CMOS process. The power consumption is only $5.2\mu\text{W}$ per channel with a 3.3V supply and 200 kHz reference clock. The compact size and low power of this circuit enable an around 150 IDC channels can be integrated in a $3\times 3\text{ mm}^2$ chip to achieve high throughput biosensor array microsystem.

C. Implemented the first ever single-chip thermal control and impedance detection microsystem for protein biosensor arrays.

The first to merge the thermal control capabilities with impedance detection instrumentation circuits into a single-chip microsystem that permits the high throughput

protein array application. The thermal controlled microsystem increases the sensitivity of biosensor reaction signals, minimizes reagent cost and a reduced time and labors.

6.2 Future Work

This work demonstrates the design of the design of a thermal controlled instrument for protein array, which can characterize the structure and function of protein and control the protein sites temperature locally. Based on the results in this thesis, there are some promising research directions for future research.

A: Combination thermal control microsystem with a temperature sensitive protein

The impedance extract circuit was already tested with tBLM protein sensor, then combination the developed thermal controlled platform with temperature sensitive protein is the next step. The study of a temperature sensitive protein, NEST, (a hydrophobic recombinant polypeptide comprising the catalytic domain (residues 727–1216) of neuropathy target esterase) is in progress. We are working on to coat the NEST protein sites on the gold electrodes interface and build a microfluidic system on top of the thermal control chip.

B: Extension to amperometric potentiostat

Beside impedance spectroscopy, amperometric potentiostat is another popular technique used for electrochemical biosensors. Our lab already developed several versions potentiostat circuits fitting for different cyclic voltammetry applications. One

reported potentiostat chip [50] includes a waveform generator, biasing potentiostats and amperometric readout circuits to support up to four channels in a sensor array, and its amperometric readout circuits achieves with a 100 μA range and a 1pA linear resolution. Another paper presented a bipotentiostat structure, which can supports redox recycling through a common potential control unit and two readout channels where excitation signals can be inserted [44]. Thanks to all these works, it is easy to migrate the existed amperometric potentiostats with the developed microsystem in this thesis into one system.

BIBLIOGRAPHY

BIBLIOGRAPHY

- [1] S. Stovall, "Scientists Reach Midpoint of Protein Study," in *The Wall Street Journal*, 2010.
- [2] Wikipedia, 2010.
- [3] J. Drews, "Drug Discovery: A Historical Perspective," *Science*, vol. 287, pp. 1960-1964, 2000.
- [4] "Global Cancer Facts & Figures 2007," 2007.
- [5] D. J. H. A. Manz, E. Verpoorte, H. M. Widmer, "Planar chips technology for miniaturization of separation systems: a developing perspective in chemical monitoring," *Advances in chromatography*, vol. 33, pp. 1-66, 1993.
- [6] A. M. G. H. W. Sanders, "Chip-based microsystems for genomic and proteomic analysis," *Trends in analytical chemistry*, vol. 19, pp. 364-378, 2000.
- [7] E. Verpoorte, "Microfluidic chips for clinical and forensic analysis," *Electrophoresis*, vol. 23, pp. 677-712, 2002.
- [8] S. C. Yang Liu, and Evangelyn C. Alcocilja, "Fundamental Building Blocks for Molecular Bio-wire based Forward-error Correcting Biosensors," *Nanotechnology*, vol. 18, pp. 424017(6pp), 2007.
- [9] I. Malsch, "Protein research calls for advanced instruments," *The Industrial physicist* pp. 18-23, 2008.
- [10] D. J. Cahill, "Protein arrays: a high-throughput solution for proteomics research?," *Proteomics: A Trends Guide*, pp. 47-51, 2000.
- [11] S. J. Maerkl, "Next generation microfluidic platforms for high-throughput protein biochemistry," *Current Opinion in Biotechnology*, vol. 22, pp. 1-7, 2010.
- [12] J. Wang, "Electrochemical biosensors: Towards point-of-care cancer diagnostics," *Biosensors and Bioelectronics*, vol. 21, pp. 1887-1892, 2006.
- [13] A. Bard, and L. Faulkner, *Electrochemical Methods: Fundamentals and Applications*, 2nd ed. New York: John Wiley & Sons, 2001.

- [14] N. K. B. L. Hassler, J. G. Zeikus, Lee, I. Worden, R. M., "Renewable dehydrogenase-based interfaces for bioelectronic applications," *Langmuir*, vol. 23, pp. 7127-7133, 2007.
- [15] S. Y. R. R. Sathuluri, E. i. Tamiya, "Microsystems Technology and Biosensing " *Advances in Biochemical Engineering/Biotechnology*, vol. 109, pp. 285-350, 2008.
- [16] C. W. L. C. Yi, S. Ji, M. Yang, "Microfluidics technology for manipulation and analysis of biological cells," *Analytica Chimica Acta*, vol. 560, pp. 1-23, 2006.
- [17] C. Yang, Y. Huang, B. L. Hassler, R. M. Worden, and A. J. Mason, "Amperometric Electrochemical Microsystem for a Miniaturized Protein Biosensor Array," *IEEE Trans. Biomedical Circ. Systems*, vol. 3, pp. 160-168, 2009.
- [18] D. R. X. Liu, A. Mason, "A fully integrated multi-channel impedance extraction circuit for biosensor arrays," presented at IEEE Int. Symp. Circuits and Systems, 2010.
- [19] J. H. A. M. Im, J. Han, T. J. Park, S. Y. Lee, and Y. Choi, "Development of a Point-of-Care Testing Platform With a Nanogap-Embedded Separated Double-Gate Field Effect Transistor Array and Its Readout System for Detection of Avian Influenza," *IEEE SENSORS JOURNAL*, vol. 11, pp. 351 - 360, 2011.
- [20] S. K. M. M. Graf, D. Barretino, and A. Hierlemann, "Transistor heater for micro-hotplate-based metal-oxide microsensors," *IEEE Electron Device Lett.*, vol. 26, pp. 295–297, 2005.
- [21] R. E. C. S. Semancik, M. C. Wheeler, J. E. Tiffany, G. E. Poirier, R. M. Walton, J. S. Suehle, B. Panchapakesan, D. L. DeVoe, "Microhotplate platforms for chemical sensor research," *Sensors and Actuators*, vol. B77, pp. 579-591, 2001.
- [22] A. Hierlemann, *Integrated Chemical Microsensor Systems in CMOS Technology*: Springer, 2005.
- [23] D. B. J. Courbat, N.F. de Rooij, "Reliability improvement of suspended platinum-based micro-heating elements," *Sensors and Actuators A*, vol. 142, pp. 284–291, 2008.
- [24] D. S. M. Malfatti, A. Simoni, L. Lorenzelli, A. Adami, A. Baschiroto, "A CMOS Interface for a Gas-Sensor Array with a 0.5%-Linearity over 500k Ω -to-1G Ω Range and $\pm 2.5^{\circ}\text{C}$ Temperature Control Accuracy," presented at IEEE International Solid-State Circuits Conference, 2006.

- [25] K. A. A. M. M. A. P. Pertijs, and J. H. Huijsing, "A CMOS smart temperature sensor with a 3σ inaccuracy of ± 1 °C from -55 °C to 125 °C," *IEEE J. Solid-State Circuits*, vol. 40, pp. 2805–2815, 2005.
- [26] M. A. P. P. A. L. Aita, K. A. A. Makinwa, and J. H. Huijsing, "A CMOS smart temperature sensor with a batch-calibrated inaccuracy of ± 0.25 °C (3σ) from -70 °C to 130 °C," *Dig. Tech. Papers ISSCC*, pp. 342–343, 2009.
- [27] L. J. B. F. Sebastiano, K. A. Makinwa, S. Drago, D. M. Leenaerts, and B. Nauta, "A 1.2 V 10 μ W NPN-based temperature sensor in 65 nm CMOS with an inaccuracy of ± 0.2 °C (3σ) from -70 °C to 125 °C," in *Dig. Tech. Papers ISSCC*, pp. 312-313, 2010.
- [28] R. E. C. J. Suehle, M. Gaitan, S. semancik, "Tin oxide gas sensor fabricated using CMOS micro-hotplates and in situ processing," *IEEE Electron Device Lett.*, pp. 118-120, 1993.
- [29] K. D. W. N. Najafi, R. Merchante, J. W. Schwank, "An intergrated multi-element ultrathin film gas analyzer," *IEEE Workshop on Sensors and Actuators*, pp. 19-22, 1992.
- [30] K. D. W. N. Najafi, J. W. Schwank, "A micromachined ultra-thin-film gas detector," *IEEE Trans. Electron Devices*, pp. 1770-1777, 1994.
- [31] V. N. B. Samel, A. Russom, P. Griss, G. Stemne, "A disposable lab-on-a-chip platform with embedded fluid actuators for active nanoliter liquid handling," *Biomed Microdevices*, vol. 9, pp. 61-67, 2007.
- [32] J. M. R. Casanova, L. Dieguez, S.A. Bota and J. Samitier, "A mixed-mode temperature control circuit for gas sensors," presented at IEEE Int. Symp. Circuits and Systems,, 2004.
- [33] M. G. U. Frey, S. Taschini, K. U. Kirstein, and A. Hierlemann, "A Digital CMOS Architecture for a Micro-Hotplate Array," *IEEE J. Solid-State Circuits*, vol. 42, pp. 441-450, 2007.
- [34] Y. L. C. Lee, H. Shieh, C. Tong, "LabVIEW Implementation of an Auto-tuning PID Regulator via Grey-predictor," presented at IEEE Cybernetics and Intelligent Systems Conference 2006.
- [35] P. M. D. Barrettino, M. Graf, S. Hafizovic, A. Hierlemann, "CMOS-Based Monolithic Controllers for Smart Sensors Comprising Micromembranes and Microcantilevers," *EEE TRANSACTIONS ON CIRCUITS AND SYSTEMS—I: REGULAR PAPERS*, vol. 54, pp. 141-152, 2007.

- [36] B. L. D. Barrettino, M. E. Martin, S. McQuaide, D. Meldrum, "CMOS Readout and Control Architecture for Single-Cell Real-Time Microsystems," presented at IEEE International Symposium Circuits and Systems, 2005.
- [37] D. W. P. F. D. Braun, T. A. Papalias, "On-Chip Temperature Control Circuit Using Common Devices," presented at IEEE Custom Integrated Circuits Conf., 2005.
- [38] B. J. N. Bhat, R. Pratap, S. Bagga, S. Mohan, "Integrated CMOS Gas Sensors," presented at 2009 2nd International Workshop on Electron Devices and Semiconductor Technology, 2009.
- [39] M. G. A. Lombardi, L. Bruno, P. Malcovati, A. Baschiroto, "A Fully Integrated Interface Circuit for 1.5°C Accuracy Temperature Control and 130-dB Dynamic-Range Read-Out of MOX Gas Sensors," *Solid-State Circuits Conference, European*, pp. 78-81, 2008.
- [40] M. M. a. T. Parve, "Improvement of Lock-in Bioimpedance Analyzer for Implantable Medical Devices," *IEEE Trans. Instrum. Meas.*, vol. 56, pp. 968-974, 2007.
- [41] G. F. F. Gozzini, M. Sampietro, "An Instrumenton-chip for Impedance Measurements on Nanobiosensors with AttoFarad Resolution," presented at IEEE Int. Conf. Solid State Circ., 2009.
- [42] A. R. A. Yúfera, J. M. Muñoz, R. Doldán, G. Leger, "A Tissue Impedance Measurement Chip for Myocardial Ischemia Detection," *IEEE Trans. Circ. Syst.*, vol. 52, pp. 2620-2628, 2005.
- [43] L. R. F. A. J. Bard, *Elelctrochemical Methods*. NewYork: Wiley, 1980.
- [44] Y. Huang and A. J. Mason, "A Redox-Enzyme-Based Electrochemical Biosensor with a CMOS Integrated Bipotentiostat," presented at IEEE BioCAS Conf., 2009.
- [45] X. Liu, L. Li, and A. J. Mason, "Thermal Control Microsystem for Protein Characterization and Sensing," presented at IEEE BioCAS Conf., 2009.
- [46] A. G. A. J. Christen, "Design, fabrication, and testing of a hybrid CMOS/PDMS microsystem for cell culture and incubation," *IEEE Trans. On biomedical circuits and systems*, vol. 1, pp. 3-18, 2007.
- [47] N. Dotson, "A Post-CMOS Thermally Controlled Biosensor Array Microsystem," in *ECE*, vol. Master: Michigan State University, 2004.

- [48] N. Trombly and A. Mason, "Post-CMOS electrode formation and isolation for on-chip temperature-controlled electrochemical sensors," *IET Electronics Letters*, vol. 44, pp. 29-30, 2008.
- [49] N. Trombly, "Electrical and Thermal Interfaces for On-chip Electrochemical Biosensor Arrays," in *ECE*, vol. Master: Michigan State University, 2006.
- [50] L. Li, W. A. Qureshi, X. Liu, and A. J. Mason, "Amperometric Instrumentation System with on-chip Electrode Array for Biosensor Application," presented at IEEE Conf. Biomedical Circuits and Systems, 2010.
- [51] M. van Tienhoven, J. Atkins, Y. Li, and P. Glynn, "Human neuropathy target esterase catalyzes hydrolysis of membrane lipids," *Journal of Biological Chemistry*, vol. 277, pp. 20942-20948, 2002.
- [52] X. Zhu and C. H. Ahn, "On-chip electrochemical analysis system using nanoelectrodes and bioelectronic CMOS chip," *IEEE Sensors J.*, vol. 6, pp. 1280-1286, 2006.
- [53] R. N. S. G. S. Popkirov, "A New Impedance Spectrometer for the Investigation of Electrochemical Systems," *Review of Scientific Instruments*, vol. 61, pp. 5366-5372, 1992.
- [54] O. M. M. Min, T. Parve, "Lock-in Measurement of Bio-Impedance Variations," *Measurement*, vol. 27, pp. 21-28, 2000.
- [55] T. P. M. Min, "Improvement of Lock-in Bio-impedance Analyzer for Implantable Medical Devices," *IEEE Trans. Instrum. Meas.*, vol. 56, pp. 968-974, 2007.
- [56] C. Yang, S. R. Jadhav, R. M. Worden, and A. J. Mason, "Compact Low-Power Impedance-to-Digital Converter for Sensor Array Microsystems," *IEEE J. Solid State Circuits*, vol. 44, pp. 2844-2855, 2009.
- [57] E. A. Vittoz and O. Neyroud, "A Low- voltage CMOS Bandgap Reference " *IEEE, JSSC*, vol. 14, pp. 573-579, 1979.
- [58] D. Barrettino, M. Graf, M. Zimmermann, C. Hagleitner, A. Hierlemann, and H. Baltes, "A Smart Single-Chip Micro-Hotplate-Based Gas Sensor System in CMOS-Technology," *Analog Integrated Circuits and Signal Processing*, vol. 39, pp. 275-287, 2004.
- [59] F. Serra-Graells and J. L. Huertas, "Sub-1-V CMOS proportional-to-absolute temperature references," *JSSC*, vol. 38, pp. 84 - 88, 2003.

- [60] R. M. W. B. Hassler, A. Mason, P. Kim, N. Kohli, J. G. Zeikus, et al., "Biomimetic interfaces for a multifunctional biosensor array microsystem," presented at IEEE Int. Conf. on Sensors, Vienna, Austria, 2004.
- [61] V. Atanasov, N. Knorr, R. S. Duran, S. Ingebrandt, A. Offenhausser, W. Knoll, and I. Koper, "Membrane on a chip: A functional tethered lipid bilayer membrane on silicon oxide surfaces," *Biophysical Journal*, vol. 89, pp. 1780-1788, 2005.
- [62] B. Raguse, V. Braach-Maksvytis, B. A. Cornell, L. G. King, P. D. J. Osman, R. J. Pace, and L. Wiczorek, "Tethered lipid bilayer membranes: Formation and ionic reservoir characterization," *Langmuir*, vol. 14, pp. 648-659, 1998.